B cells imprinted by ancestral SARS-CoV-2 develop pan-sarbecovirus neutralization in immune recalls

Xixian Chen[1,2,#], Ling Li[1,#], Ruiping Du[1,2,#], Zuowei Wang[1,#], Yunjian Li[1,2], Yi Sun[1,2], Rongrong Qin[1,2], Hualong Feng[1], Lin Hu[1], Xuanyi Chen[1], Maosheng Lu[1], Xueyan Huang[1], Liwei Jiang[1,*], Teng Zuo[1,*]

[1]Laboratory of Immunoengineering, Institute of Health and Medical Technology, Hefei Institutes of Physical Science, Chinese Academy of Sciences, Hefei 230031, China

[2]University of Science and Technology of China, Hefei 230026, China

[#]These authors contributed equally to this work

*Correspondence: jlw0531@cmpt.ac.cn (L.J.); zuot@cmpt.ac.cn (T.Z.)

Short running title: Evolution of B cells imprinted by ancestral SARS-CoV-2

Summary

Chen et al. demonstrate that B cells imprinted by ancestral SARS-CoV-2 have tremendous potential to develop neutralizing breadth and potency in repeated immune recalls driven by Omicron variants, implicating that ancestral SARS-CoV-2 immune imprinting can be harnessed in developing pan-SARS-CoV-2 and even pan-sarbecovirus vaccines.

Abstract

A key question on ancestral SARS-CoV-2 immune imprinting is to what extent imprinted B cells can develop neutralizing breadth and potency in immune recalls. Here, we longitudinally tracked B cells recognizing wild-type spike in two individuals, who were sequentially infected by Omicron variants after receiving mRNA vaccines. Functional and genetic analysis of 632 monoclonal antibodies (mAbs) from those B cells reveals that mAbs cloned after second infection have dramatically enhanced neutralizing breadth and potency, which is attributed to recall and maturation of pre-existing memory B cells. Among the 11 mAbs that potently neutralize SARS-CoV-2 variants from wild-type to KP.3, 5 mAbs are classified into public clonotypes encoded by IGHV3-53 or IGHV3-66, whereas the rest belong to a rarely reported clonotype encoded by IGHV3-74. Notably, IGHV3-74 mAbs can also broadly neutralize other sarbecoviruses by targeting a novel epitope on receptor-binding domain of spike. These results support that ancestral SARS-CoV-2 immune imprinting can be harnessed in developing pan-SARS-CoV-2 and even pan-sarbecovirus vaccines.

Introduction

Adaptive immune system adopts multiple mechanisms to ensure specific and diverse antibody responses against various pathogens. During B cell development, V(D)J recombination generates a vast diversity of B cell antigen receptors (BCRs) for naïve B cells (Tonegawa, 1983). When infection or vaccination occurs, a small portion of naïve B cell repertoire get activated as their BCRs recognize corresponding antigens by chance (Batista and Harwood, 2009). Activated B cells either differentiate into short-lived plasmablasts (PBs) to produce the initial wave of antibodies, or enter germinal centers (GCs) to undergo repeated rounds of somatic hypermutation and affinity-dependent selection, a process known as antibody affinity maturation (Victora and Nussenzweig, 2022). The evolved GC B cells eventually differentiate into long-lived plasma cells (PCs) to constantly secrete antibodies for months to years, or memory B cells to wait for future encounter with the same or similar antigens (Victora and Nussenzweig, 2022). Compared with primary antigen exposure, secondary antigen exposure typically leads to much faster and stronger antibody responses as recalled memory B cells rapidly differentiate into PB/PCs to secrete high-affinity antibodies (Inoue et al., 2018). In addition, memory B cells can be recruited into newly formed GCs to further mature upon secondary antigen exposure (Inoue et al., 2018). Overall, these mechanisms work in concert to establish antibody-mediated immune protection against infections.

Since the outbreak of SARS-CoV-2, numerous studies on human antibody responses against spike protein of this emerging virus have been conducted to inform the development of vaccines and antibody therapeutics (Lapuente et al., 2024; Qi et al., 2022; Roltgen and Boyd, 2024). Early in the pandemic, extensive isolation and characterization of monoclonal antibodies (mAbs) from convalescents reveals that neutralizing antibodies primarily target epitopes on receptor-binding

56 domain (RBD) and to a lesser extent on N-terminal domain (NTD) of spike (Ling et al., 2023; Liu and
57 Wilson, 2022). Furthermore, RBD-specific neutralizing antibodies are categorized into seven major
58 groups according to their binding modes and fine epitopes (Hastie et al., 2021), whereas NTD-specific
59 neutralizing antibodies largely target a single supersite (Cerutti et al., 2021; McCallum et al., 2021).
60 Although spike-specific antibodies from different convalescents are highly diverse, a series of public
61 antibodies (i.e. antibodies generated by different individuals while sharing common genes and antigen
62 recognition modes) have been widely reported, including antibodies encoded by IGHV3-53, IGHV3-
63 66, IGHV1-58 and IGHV1-69 (Robbiani et al., 2020; Wang et al., 2022a; Yan et al., 2022; Yuan et al.,
64 2020a). In addition, longitudinal profiling of memory B cells from peripheral blood of convalescents
65 demonstrates that spike- or RBD-specific memory B cells display increased somatic hypermutation,
66 binding affinity and neutralizing potency over time, reflecting long-lasting GC responses elicited by
67 primary SARS-CoV-2 infection (Gaebler et al., 2021; Sakharkar et al., 2021; Sokal et al., 2021).
68 Compared with SARS-CoV-2 infection, two doses of SARS-CoV-2 mRNA vaccines lead to equivalent
69 plasma neutralizing activity and similar amount of RBD-specific memory B cells (Wang et al., 2021).
70 Spike- or RBD-specific mAbs cloned from vaccinees and convalescents recognize common epitopes
71 and share frequently-used antibody genes (Wang et al., 2021). Moreover, analysis of draining lymph
72 node samples from vaccinees indicates that mRNA vaccines provoke persistent GCs, which last for
73 at least six months and enable the maturation of spike-specific B cells (Kim et al., 2022; Turner et al.,
74 2021).

75 Under the immune pressure established by infection and vaccination, SARS-CoV-2 variants,
76 represented by Alpha (B.1.1.7), Beta (B.1.351), Gamma (P.1), Delta (B.1.617.2) and Omicron
77 (B.1.1.529), emerged successively in the first two years of the pandemic. Among them, Omicron

78 exhibited most striking evasion to neutralizing antibodies induced by ancestral SARS-CoV-2 spike
79 and therefore caused a new wave of infections worldwide (Viana et al., 2022). Omicron infection in
80 individuals administrated with mRNA vaccines predominantly recalls cross-reactive memory B cells
81 elicited by vaccination whereas rarely induces *de novo* Omicron-specific B cells responses,
82 highlighting that ancestral SARS-CoV-2 imprints B cell responses to Omicron (Kaku et al., 2022;
83 Quandt et al., 2022; Wang et al., 2022b; Weber et al., 2023). Consequently, plasma neutralizing
84 activity against ancestral SARS-CoV-2 and Omicron are enhanced synchronously (Kaku et al., 2022;
85 Quandt et al., 2022; Wang et al., 2022b; Weber et al., 2023). Moreover, B cell clones with more
86 mutations and higher affinities towards Omicron progressively remodel spike-specific memory B cell
87 repertoire, suggesting that cross-reactive memory B cells can undergo further affinity maturation in
88 new GCs induced by Omicron breakthrough infection (Kaku et al., 2023; Sokal et al., 2023).
89 With the rapid emergence of Omicron-derived variants, such as BA.2.75, BA.5, BF.7, BQ.1, XBB.1.5,
90 XBB.1.16, EG.5.1, BA.2.86 and JN.1, repeated infections with these variants have become common
91 and updated vaccines have been applied accordingly in some countries (Huang et al., 2023). In
92 individuals with prior exposures to wild-type (WT) spike, antibody responses boosted by subsequent
93 exposures to emerging Omicron variants, either through infection or vaccination, display biased
94 neutralizing activities to ancestral SARS-CoV-2 and earlier Omicron variants, suggesting that immune
95 imprinting may impede the elicitation of neutralizing antibodies against more recent and future variants
96 (Johnston et al., 2024; Liang et al., 2024; Tortorici et al., 2024; Wang et al., 2023a; Yisimayi et al.,
97 2024). Nonetheless, mAbs from those individuals dramatically surpass mAbs elicited by WT spike in
98 neutralizing breadth and potency, indicating that immune imprinting is potentially beneficial for the
99 development of broadly neutralizing antibodies (bnAbs) (Paciello et al., 2024; Sokal et al., 2023).

100 To better understand the beneficial effects of ancestral SARS-CoV-2 immune imprinting on antibody
101 responses to emerging variants, we ask that to what extent imprinted B cells (i.e. memory B cells
102 elicited by ancestral SARS-CoV-2) can develop neutralizing breadth and potency in immune recalls.
103 To address this question, we performed a 7-month longitudinal study of B cells recognizing WT spike
104 in two individuals of mRNA vaccine, from convalescence of breakthrough infection to acute phase of
105 reinfection. Functional and genetic analysis of 632 mAbs from those B cells reveals that mAbs cloned
106 after reinfection have dramatically enhanced neutralizing breadth and potency, which is attributed to
107 recall of pre-existing memory B cells and maturation of those cells either before or after reinfection.
108 Among the 11 mAbs that potently neutralize all tested SARS-CoV-2 variants from WT to KP.3, 5 mAbs
109 are classified into public clonotypes encoded by IGHV3-53 or IGHV3-66, whereas the rest belong to
110 a rarely reported clonotype encoded by IGHV3-74. Notably, IGHV3-74 mAbs can also broadly
111 neutralize a panel of sarbecoviruses including SARS-CoV-1, Pangolin CoV GD, Bat CoV WIV16 and
112 RaTG13. Structural and functional analysis shows that IGHV3-74 mAbs can block the binding
113 between RBD and ACE2 by targeting a novel epitope consisting of E340-R346, V367-S375, N436-
114 G446 and Q498-V503. Moreover, the best IGHV3-74 mAb, termed KXD355, is highly resilient to
115 variations on this epitope. Overall, this study demonstrates that both public and rare antibody
116 clonotypes imprinted by ancestral SARS-CoV-2 have potential to achieve extraordinary neutralizing
117 breadth and potency in repeated Omicron infections, which implicates that ancestral SARS-CoV-2
118 immune imprinting can be harnessed in developing pan-SARS-CoV-2 and even pan-sarbecovirus
119 vaccines.

120 **Results**

121 **Reinfection enhances plasma neutralizing antibody responses**

122 In our previous study, we recruited a cohort to study antibody responses elicited by breakthrough
123 infection (Li et al., 2023). Among them, Donor 1 and 2 received two doses of mRNA vaccines in the
124 middle or beginning of 2021 and were infected by BA.5 or BF.7 in the end of 2022 (Figure 1A). With
125 their blood samples collected about two months (T1) after infection, we have identified multiple mAbs
126 with broadly neutralizing capacity (Li et al., 2023). To longitudinally track B cell responses in these
127 two donors, we also collected blood samples about 3 months (T2) and 6 months (T3) after infection.
128 Donor 1 showed symptoms of infection and was confirmed by SARS-CoV-2 antigen test on August
129 25, 2023, when EG.5.1 caused a new round of infections in China (Wang et al., 2023b). Eleven days
130 later (T4), blood was collected again from Donor 1 to study acute phase antibody responses evoked
131 by reinfection. In parallel, we also collected blood from Donor 2 at T4, though Donor 2 reported no
132 symptoms and negative test results during several waves of infections before this time point.
133 We measured neutralizing antibody titers of plasma from four time points against a panel of 18
134 pseudoviruses bearing spikes from ancestral SARS-CoV-2 (WT), Alpha, Beta, Gamma, Delta, BA.1,
135 BA.4/5, BA.2.75, BQ.1, XBB, XBB.1.5, EG.5.1, HK.3, BA.2.86, JN.1, KP.2, KP.3 and SARS-CoV-1
136 (Figure 1B and Figure S1). Overall, the plasma neutralizing titers (NT50s) of both donors gradually
137 decrease from T1 to T3 with a maximum of 10.7 folds. After reinfection, plasma from Donor 1 at T4
138 shows substantially increased neutralizing titers against most strains by a maximum of 20.7 folds
139 compared to T3. The titers of plasma from Donor 2 continuously decline or sustain from T3 to T4 for
140 most strains, whereas increase by 1.9 to 2.7 folds for strains including Gamma, BA.1 and XBB. As
141 latest variants of XBB and BA.2.86 lineages, HK.3 and KP.3 are least sensitive to neutralization,
142 highlighting the continuous neutralization escape (Figure 1C). Nonetheless, plasma at T4 from Donor

143 1 displays relatively stable neutralizing titers across all SARS-CoV-2 variants, indicating that
144 reinfection enhances the breadth of neutralizing antibody response in Donor 1.

145 **Monoclonal antibodies cloned from WT-spike-specific B cells after reinfection exhibit**
146 **improved neutralizing breadth and potency**

147 As B cells imprinted by ancestral SARS-CoV-2 mRNA vaccine (i.e. memory B cells) typically maintain
148 their specificities to WT spike in recalled responses (Johnston et al., 2024; Kaku et al., 2022; Kaku et
149 al., 2023; Liang et al., 2024; Quandt et al., 2022; Sokal et al., 2023; Tortorici et al., 2024; Wang et al.,
150 2023a; Wang et al., 2022b; Weber et al., 2023; Yisimayi et al., 2024), we used WT spike as bait to
151 track imprinted B cells in peripheral blood mononuclear cells (PBMCs) from these two donors.
152 Consistent with plasma neutralizing titers, the frequencies of WT-spike-specific B cells in Donor 1
153 drop sequentially from T1 to T3 and then rise back to initial level (Figure 2A). Unexpectedly, Donor 2
154 displays similar dynamic changes as Donor 1, suggesting that Donor 2 may have experienced an
155 asymptomatic infection between T3 and T4.

156 To examine the binding and neutralizing properties of antibodies from those WT-spike-specific B
157 cells, we cloned the variable regions of antibodies from those B cells into expression vectors through
158 single-cell RT-PCR. Then we transfected HEK293T cells with those vectors and harvested
159 supernatant for ELISA and neutralization assay (Figure 2B). In ELISA, the supernatant was tested
160 with RBD, NTD, S1, S2 and spike (S) from WT SARS-CoV-2 and spikes from Omicron variants
161 including BA.4/5, XBB.1.5, EG.5.1 and JN.1. In neutralization assay, the supernatant was tested
162 against WT, BA.4/5, XBB.1.5, EG.5.1 and JN.1 pseudoviruses.

163 With published mAbs at T1 included, we identified 448 and 184 WT-spike-specific mAbs from Donor
164 1 and Donor 2 respectively. The main targets of these mAbs are RBD, NTD and S2, with the

165 proportions of mAbs to each domain slightly varying from T1 to T4 (Figure 2C). Regarding to cross-
166 binding with different spikes, the frequencies of RBD-specific mAbs that bind WT and one Omicron
167 variant, either BA.4/5, XBB.1.5, EG.5.1 or JN.1, decline from T1 to T3 and then ascend (Figure 2D,
168 Figure S2A). However, similar trend is not observed in NTD- and S2-specific mAbs.

169 By defining 70% inhibition as cutoff, we identified 127 mAbs that are able to neutralize WT
170 pseudoviruses (WT-neutralizing mAbs), with 77 from Donor 1 and 50 from Donor 2 (Figure 2E).
171 Among them, only 5 mAbs target NTD while the others exclusively recognize RBD. Regarding to
172 cross-neutralizing activity, around 20-30% of mAbs at T4 are able to neutralize all 5 tested
173 pseudoviruses, whereas only 2 out of 61 mAbs from T1 to T3 have such capacity (Figure 2F).
174 Moreover, the frequencies of mAbs that cross-neutralize WT and one Omicron variant drop from T1
175 to T3 and then jump to highest levels at T4 (Figure 2G, Figure S2B).

176 To further compare the breadth and potency of neutralizing mAbs from different time points, we
177 purified those mAbs and measured their IC50s against 14 representative pseudoviruses including
178 WT, Delta, BA.1, BA.4/5, BA.2.75, BQ.1, XBB.1.5, EG.5.1, HK.3, BA.2.86, JN.1, KP.2, KP.3 and
179 SARS-CoV-1 (Figure 3A). Four neutralizing mAbs screened by supernatant were not included in this
180 analysis because of low yields. Among all tested mAbs, 4 mAbs from Donor 2 are able to neutralize
181 all SARS-CoV-2 variants and SARS-CoV-1. In addition, 2 mAbs from Donor 1 and 5 mAbs from Donor
182 2 can neutralize all SARS-CoV-2 variants from WT to KP.3. Notably, these 11 mAbs are exclusively
183 identified from PBMCs collected at T4. Along with this finding, differences are observed in the overall
184 neutralizing breadth of mAbs at T1 to T4 (Figure 3B, Figure S3A). T1 and T4 have higher frequencies
185 of neutralizing antibody against BA.1, BA.4/5, BA.2.75, BQ.1, XBB.1.5 and BA.2.86 than T2 and T3,

186 which is consistent with neutralization results of supernatant. Moreover, T4 has higher proportions of
187 neutralizing antibody against EG.5.1, HK.3, JN.1, KP.2 and KP.3 than the other time points.
188 Regarding to neutralizing potency, the overall IC50s of mAbs at T4 are lower than that of mAbs at
189 T2 and T3 against most strains (Figure 3C, D, Figure S3A). In addition, mAbs at T4 also display
190 superior neutralizing potency than mAbs at T1 against Delta, EG.5.1, HK.3, JN.1 and KP.2. In contrast,
191 significant differences in IC50s are generally not observed among mAbs at T1 to T3 by statistical
192 analysis. We also combined mAbs at T1 to T3 together and compared them with mAbs at T4, which
193 further confirms that mAbs isolated after reinfection have superior neutralizing breadth and potency
194 than mAbs before reinfection (Figure S3B-D). Taken together, these data suggest that mAbs cloned
195 from WT-spike-specific B cells after reinfection have enhanced neutralizing breadth and potency.
196 **Reinfection recalls pre-existing memory B cells**
197 To explain the enhanced neutralizing breadth and potency of mAbs cloned after reinfection, we moved
198 on to analyze the sequences of mAbs from T1 to T4. Binding mAbs from both donors use a wide
199 range of V genes (Figure 4A, B). The frequencies of each V gene from T1 to T4 are more consistent
200 for mAbs from Donor 1 than those from Donor 2, likely due to fewer mAbs isolated from Donor 2 at
201 T2 and T3. The most frequently-used V genes for heavy chain include IGHV3-30, IGHV3-66, IGHV3-
202 53, IGHV3-33, IGHV1-69 and IGHV1-46. Among them, IGHV3-30 and IGHV3-33 are primarily used
203 by mAbs targeting S2, whereas IGHV3-66, IGHV3-53 and IGHV1-69 are preferentially used by mAbs
204 recognizing RBD (Figure S4A). The most frequently-used V genes for light chain include IGKV1-39,
205 IGKV3-20, IGKV3-15, IGKV3-11, IGKV1-33, IGKV1-5 and IGKV1-9, which are less biased toward
206 mAbs targeting a certain domain than V genes for heavy chain (Figure S4A). In contrast to binding
207 mAbs, neutralizing mAbs are predominantly encoded by IGHV3-66, IGHV3-53 and IGHV1-69 (Figure

208 4A, B). Furthermore, in these neutralizing mAbs, IGHV3-66 and IGHV3-53 typically pair with IGKV1-
209 33, IGKV1-9 and IGKV3-20, whereas IGHV1-69 commonly pair with IGLV1-40 (Figure S4B). It is
210 worth mentioning that the pair of IGHV3-74 and IGKV3-20 is used by 10 out of 50 neutralizing mAbs
211 from Donor 2. Nonetheless, the overall profiles of V gene usage are rather consistent from T1 to T4.

212 According to V and J genes and CDR3 similarity, we defined 401 and 145 unique clonotypes
213 respectively from 448 and 184 mAbs (Figure 4C). The expanded clonotypes are primarily found in
214 mAbs at T4, particular for Donor 2, further indicating that T4 is also in acute phase of reinfection for
215 Donor 2. As an evidence of recall of pre-existing memory B cells, multiple clonotypes found at T1 to
216 T3 are extensively expanded at T4, particular for neutralizing clonotypes such as Clonotype 204 and
217 223 from Donor 1 and Clonotype 88 and 92 from Donor 2 (Figure 4D).

218 On the other hand, mAbs at T4 have more somatic mutations than those from earlier time points,
219 which can be either due to recall of pre-existing memory B cells with more mutations, or due to further
220 maturation of pre-existing memory B cells in new GC reactions (Figure 4E). Taken together, these
221 data suggest that the enhanced neutralizing breadth and potency of mAbs at T4 is attributed to recall
222 of pre-existing memory B cells and maturation of those cells either before or after reinfection.

223 **Both public and rare antibody clonotypes can develop extraordinary neutralizing breadth and**
224 **potency**

225 After longitudinal analysis of overall B cell responses in these two donors, we moved on to
226 characterize the 11 mAbs with extraordinary neutralizing breadth (Figure 3A, Figure 5A). Clonotype
227 analysis reveals that they belong to 5 unique clonotypes including Clonotype 92, 82 and 75 from
228 Donor 2 and Clonotype 240-2 and 212-1 from Donor 1. Clonotype 92 is encoded by IGHV3-74 and
229 IGHV3-20, which is rarely reported in RBD-specific antibodies against SARS-CoV-2 (Wang et al.,

230 2022a). This clonotype contains 10 neutralizing mAbs, with 1 from T2 and 9 from T4. Among them,
231 KXD350, KXD352, KXD355 and KXD358 can neutralize all tested SARS-CoV-2 variants and SARS-
232 CoV-1. Further neutralization analysis shows that KXD350 and KXD355 can also neutralize other
233 sarbecoviruses including Pangolin CoV GD, Bat CoV WIV16 and RaTG13-T372A, whereas KXD352
234 and KXD358 are escaped by RaTG13-T372A (Figure 5B). According to the phylogenetic tree, mAbs
235 in this clonotype can be divided into two major clades, suggesting that neutralizing breadth can be
236 developed through diverse evolution pathways.

237 The other four clonotypes belong to previously defined IGHV3-53/3-66 public antibody clonotypes
238 (Wang et al., 2022a). Clonotype 82 is encoded by IGVH3-66 and IGKV1-33 and contains 8
239 neutralizing mAbs from T4. However, only KXD357 is able to neutralize all SARS-CoV-2 variants, with
240 IC50s ranging from 0.003 to 0.224 μg/ml. Similar as Clonotype 92, Clonotype 82 also has two major
241 clades. Although mAbs in both clades are extensively mutated, mAbs in Clade-2 exhibit superior
242 neutralizing breadth than mAbs in Clade-1. Encoded by IGHV3-53 and IGKV3-15, Clonotype 75
243 contains previously published KXD02 from T1 and two addition mAbs from T4. In our previous study,
244 we have shown that KXD02 broadly neutralizes SARS-CoV-2 variants from WT to HK.3 (Li et al.,
245 2023). However, KXD02 is soon escaped by variants in BA.2.86 lineages including JN.1, KP.2 and
246 KP.3. In contrast, KXD353 and KXD356 from T4 maintain neutralizing activities against all SARS-
247 CoV-2 variants, with IC50s ranging from 0.002 to 0.216 μg/ml. In line with increased neutralizing
248 breadth and potency, KXD353 and KXD356 are also more evolved than KXD02 according to
249 phylogenetic analysis. As singletons from Donor 1, Clonotype 240-2 (KXD470) is encoded by IGHV3-
250 66 and IGKV1-9, whereas Clonotype 212-1 (KXD472) is encoded by IGHV3-53 and IGKV1-5.

251 Although both mAbs are able to neutralize all SARS-CoV-2 variants, they are less potent to KP.2 and
252 KP.3 than bnAbs from Donor 2.

253 As all these clonotypes are identified with WT spike, we assume that they are initially primed by
254 ancestral SARS-CoV-2 mRNA vaccine but not by BA.5 or BF.7 breakthrough infection. To confirm
255 this assumption, we synthesized the putative germline antibodies of each clonotypes and measured
256 their binding avidities to WT and BA.4/5 spikes expressed on HEK293T cells (Figure 5C). BF.7 was
257 not tested since it has only one amino acid different from BA.5 in RBD. All the germlines, except GL-
258 4, show strong to moderate binding to WT spike. In contrast, they all display weak or even
259 undetectable binding to BA.4/5 spike. The biased recognition towards WT spike suggest that these
260 clonotypes are more likely to be activated by mRNA vaccine. Taken together, these data suggest that
261 both public and rare antibody clonotypes imprinted by ancestral SARS-CoV-2 have potential to
262 develop ultra-broad and potent neutralizing activities in repeated Omicron infections.

263 **IGHV3-74-encoded bnAbs target a novel epitope and exhibit dramatic resilience to mutations**
264 **on the epitope**

265 To evaluate the neutralizing potential of above bnAbs to future SARS-CoV-2 variants, we moved on
266 to analyze their epitopes. We first performed competition ELISA to roughly map their epitopes with
267 ACE2, CR3022, S309, P2S-2E9, BD55-5483, BD56-1854 and BD55-1205 as references (Figure 6A).
268 As reported, CR3022 binds to a cryptic epitope on the inner face of RBD whereas S309 recognizes
269 N343 proteoglycan epitope on the outer face of RBD (Figure S5A) (Pinto et al., 2020; Yuan et al.,
270 2020b). P2S-2E9 and BD55-5483 (analogue of BD55-5514) both target the previously defined “mesa”
271 of RBD, respectively biased to the outer face and inner face (Cao et al., 2022; Hastie et al., 2021; Ju

272 et al., 2023). As representatives of IGHV3-53/3-66 public antibodies, BD56-1854 and BD55-1205
273 target receptor-binding-motif (RBM) (Cao et al., 2023).

274 We tested four mAbs (KXD350, KXD352, KXD355 and KXD358) from Clonotype 92 (IGHV3-74
275 mAbs) and five mAbs (KXD353, KXD356, KXD357, KXD470 and KXD472) from other clonotypes
276 (IGHV3-53/3-66 mAbs) (Figure 6A). IGHV3-53/3-66 mAbs compete with BD55-5483, BD56-1854 and
277 BD55-1205 but not with S309 and P2S-2E9. In contrast, IGHV3-74 mAbs compete with S309, P2S-
278 2E9 and BD55-5483 while not with BD56-1854 and BD55-1205. Moreover, no competition is observed
279 between these mAbs and CR3022 except for some minor competition between KXD358 and CR3022.
280 In addition, they all compete with ACE2, suggesting that they neutralize SARS-CoV-2 through
281 receptor blockade.

282 To define the fine epitopes of these mAbs, we performed structure prediction with AlphaFold 3
283 (Abramson et al., 2024). The predicted structures of IGHV3-53/3-66 mAbs in complex with WT RBD
284 are similar to the structure of BD55-1205 in complex with XBB.1.5 RBD (Figure S5B). According to
285 these structures, we defined the common epitope of IGHV3-53/3-66 mAbs, which largely overlap with
286 the epitope of ACE2 (Figure 6B, C).

287 On the other hand, AlphaFold 3 generated various structures for the complexes of IGHV3-74 mAbs
288 and WT RBD. However, only one type of structures is consistent with epitope mapping by competition
289 ELISA. Here, KXD355 is taken as an example to present the results. Binding to the previously defined
290 “escarpment” of RBD (Hastie et al., 2021), KXD355 clashes with S309, P2S-2E9 and BD55-5514
291 (analogue of BD55-5483) but not with BD55-1205 and CR3022 (Figure S5C). As this epitope is
292 exposed on both up and down RBDs, KXD355 can bind RBDs in both conformations (Figure 6D). In
293 details, the long CDRH3 of KXD355 extends into a groove formed by three helixes on the “escarpment”

294 of RBD (Figure 6E). Meanwhile, the other CDRs attach to “mesa” of RBD to provide support for
295 CDRH3. Accordingly, the epitope of KXD355 includes 22 residues distributed on E340-R346, V367-
296 S375, W436-G446 and Q498-V503 (Figure 6F).

297 To confirm the predicted epitopes, we constructed a panel of single-mutated KP.3 spikes and
298 measured their escape to those mAbs in binding and neutralization (Figure 6G). Compared to KP.3,
299 most mutants show similar or slightly lower expression levels on HEK293T cells, which is indicated
300 by an NTD-specific mAb. In contrast, nearly half of these mutants display reduced binding to ACE by
301 different extent. Regarding to the binding with mAbs, mutants including K403D, D420N, Y421K,
302 L456V, L456S, K460F, A475V, N487K, Y489A, Y489D, R498A and R498D completely lose binding
303 to at least one IGHV3-53/3-66 mAb. To a lesser extent, mutants like N343A, N343F, K440D, L441S
304 and H445D show decreased binding to IGHV3-74 mAbs. Consistent with reduced binding, the
305 aforementioned mutants also display dramatic escape of neutralization to corresponding mAbs. In
306 addition, mutants such as T345A, T345F, K444A and K444D are also resistant to certain IGHV3-74
307 mAbs, although they only partially lose binding to those mAbs.

308 In contrast to all IGHV3-53/3-66 mAbs and other IGHV3-74 mAbs, KXD352 and KXD355 maintain
309 low IC50s against all the mutants except L441S, suggesting that they are more resilient to single
310 mutations on their epitopes (Figure S6). Compared with SARS-CoV-2 variants, SARS-CoV-1 and
311 other sarbecoviruses have multiple mutations on the epitopes of IGHV3-53/3-66 and IGHV3-74 mAbs
312 (Figure 6H). However, the best IGHV3-74 mAb, KXD355 can neutralize all the tested sarbecoviruses
313 with IC50s ranging from 0.003 to 0.151 μg/ml, further highlighting that KXD355 is highly tolerant to
314 variations on its epitope (Figure 5A, B).

315 To evaluate the likelihood that these bnAbs are escaped by future circulating SARS-CoV-2 strains,
316 we collected 25332 spike sequences published between June 1 to October 1 in 2024. With KP.3 as
317 reference, we analyzed the mutations on the epitopes of these bnAbs. With extremely low frequency,
318 multiple confirmed escape mutations for IGHV3-53/3-66 mAbs are found in the circulating strains,
319 including D420N (0.008%), A475V (0.288%), N487K (0.008%) (Figure S7A). In contrast, confirmed
320 escape mutations for IGHV3-74 mAbs are not found in the circulating strains (Figure S7B). Overall,
321 these data predict that IGHV3-74 mAbs, particular KXD355, will not be easily escaped by SARS-CoV-
322 2 in near future.

323 **Discussion**

324 The key scientific question of this study is to what extent B cells imprinted by ancestral SARS-CoV-2
325 can develop neutralizing breadth and potency in immune recalls. Strategically, we used WT spike as
326 bait to track those B cells as they typically maintain specificities to WT spike in immune recalls
327 (Johnston et al., 2024; Kaku et al., 2022; Kaku et al., 2023; Liang et al., 2024; Quandt et al., 2022;
328 Sokal et al., 2023; Tortorici et al., 2024; Wang et al., 2023a; Wang et al., 2022b; Weber et al., 2023;
329 Yisimayi et al., 2024) . A recent study pointed out that memory B cells induced by ancestral SARS-
330 CoV-2 could redirect their specificities to emerging variants in repeated Omicron exposures (Kotaki
331 et al., 2024). As our focus was memory B cells broadly recognizing SARS-CoV-2 from WT to emerging
332 variants, we did not take into account those memory B cells with redirected specificities. Regarding
333 to the samples, we collected blood from 2 individuals of mRNA vaccines at four time points, which are
334 2 months, 3 months, 6 months and 9 months after BA.5 or BF.7 breakthrough infection. In addition,
335 Donor 1 experienced a symptomatic reinfection at 11 days before the last time point, while Donor 2
336 experienced an asymptomatic reinfection shortly before the last time point, as suggested by our data.

337 Therefore, the timeline of this longitudinal study is ranging from convalescence of breakthrough
338 infection to acute phase of reinfection.

339 A major finding of this study is that mAbs cloned after reinfection have superior neutralizing breadth
340 and potency, which is accompanied with expansion of pre-existing clonotypes and increased mutation
341 levels. According to the antigen exposure history of these two donors, this finding can be explained
342 by two possibilities. First, a fraction of pre-existing memory B cells, which have already undergone
343 extensive maturation and developed superior neutralizing breadth and potency, are recalled by
344 reinfection. Second, a fraction of pre-existing memory B cells are recalled by reinfection and then
345 acquire further maturation in new GC responses. Non-mutually exclusive, these two possibilities differ
346 in whether an addition round of maturation occurs after reinfection. Previous studies suggest that
347 BA.1 breakthrough infection or booster vaccination can both lead to affinity maturation of pre-existing
348 memory B cells induced by mRNA vaccines (Alsoussi et al., 2023; Kaku et al., 2023; Sokal et al.,
349 2023). Here, it remains to be determined whether memory B cells induced by mRNA vaccines can
350 undergo two rounds of affinity maturation sequentially driven by breakthrough infection and reinfection.

351 A highlight of this study is the identification of 4 bnAbs against sarbecoviruses. These bnAbs belong
352 to a clonotype encoded by IGHV3-74, which is rarely used by RBD-specific antibodies (Wang et al.,
353 2022a). Structural analysis indicates that these IGHV3-74 bnAbs bind to an epitope consisting of
354 E340-R346, V367-S375, N436-G446 and Q498-V503. In an early study, epitopes on RBD are
355 classified into seven groups, with RBD-1 to RBD-3 on the top face, RBD-4 and RBD-5 on the outer
356 face, RBD-6 and RBD-7 on the inner face (Hastie et al., 2021). More recently, a cryptic epitope
357 recognized by human mAb BIOLS56 and IMCAS74 is defined as RBD-8 (Rao et al., 2023). Referred
358 to these epitope categories, the epitope of these IGHV3-74 bnAbs stretches across RBD-3 and RBD-

359 5 and is therefore a novel epitope. Unexpectedly, this epitope is not conserved among sarbecoviruses
360 although IGHV3-74 bnAbs can broadly neutralize those viruses. According to structures predicted by
361 AlphaFold 3, we speculate that the resilience of IGHV3-74 bnAbs to epitope variations is due to the
362 plasticity of their long CDRH3s, which play a key role in contacting with this epitope.

363 As a byproduct of defining a novel broadly neutralizing epitope on RBD, our study represents an
364 example of epitope mapping with AlphaFold 3. In our practice with AlphaFold 3, it is straightforward
365 to predict the structures of IGHV3-53/3-66 mAbs, probably because the structures of similar
366 antibodies have been abundantly reported. In contrast, various structures are predicted for IGHV3-74
367 bnAbs. In this case, traditional epitope mapping through competition ELISA is necessary to pick the
368 best candidates for further confirmation. Overall, our attempt to apply AlphaFold 3 in fine epitope
369 mapping turned out to be successful.

370 Similar to a study published recently (Jian et al., 2024), we identified multiple IGHV3-53/3-66 public
371 antibodies with ultra-broad neutralizing activities against SARS-CoV-2. In addition, we observed the
372 expansion of clonotypes encoded by IGHV3-53/3-66. According to phylogenetic analysis, the
373 improved neutralizing breadth and potency of IGHV3-53/3-66 public antibodies is somehow not
374 always correlated to the extent of somatic hypermutation, supporting the view that bystander
375 mutations generated in a stochastic manner are critical for the development of bnAbs against SARS-
376 CoV-2 (Bruhn et al., 2024; Korenkov et al., 2023). On the other hand, the neutralizing breadth of
377 IGHV3-53/3-66 public antibodies reported so far is still limited to SARS-CoV-2 variants. It remains to
378 be investigated whether this class of public antibodies can develop pan-sarbecovirus neutralization
379 after further maturation.

380 Currently, ancestral SARS-CoV-2 immune imprinting has been acknowledged as a great challenge

381 for the update of SARS-CoV-2 vaccines (Johnston et al., 2024; Liang et al., 2024; Tortorici et al., 2024;
382 Yisimayi et al., 2024). In one preprint we posted recently, we find that immune imprinting can facilitate
383 the development of bnAbs against SARS-CoV-2 (Wang et al., 2024 Preprint). Here, we further show
384 that B cells imprinted by ancestral SARS-CoV-2 can even develop pan-sarbecovirus neutralization.
385 Taken together, these studies support that ancestral SARS-CoV-2 immune imprinting can be
386 harnessed in developing pan-SARS-CoV-2 and even pan-sarbecovirus vaccines. From the aspect of
387 antibody therapeutics, KXD355 exhibits broad and potent neutralizing activity against sarbecoviruses.
388 More importantly, KXD355 targets a novel epitope and tolerates mutations on this epitope. Therefore,
389 KXD355 is an ideal candidate for antibody therapeutics against future SARS-CoV-2 variants and
390 related sarbecoviruses.

391 **Materials and methods**

392 **Ethics statement**

393 This study was approved by the Ethics Committee of Hefei Institutes of Physical Science, Chinese
394 Academy of Sciences (Approval Number: YXLL-2023-47). All donors provided written informed
395 consent for collection of information, analysis of plasma and PBMCs, and publication of data
396 generated from their samples.

397 **Human samples**

398 Peripheral blood samples were collected from 2 donors. Plasma and PBMCs were isolated from blood
399 through Ficoll density gradient centrifugation.

400 **Protein expression and purification**

401 The extracellular domains of spikes from WT, BA.4/5, XBB.1.5, EG.5.1, JN.1 were constructed with a
402 foldon-trimerization-motif, a His-tag, a tandem Strep-tag II and a FLAG-tag at C-terminal. S1, NTD

403 and RBD of WT spike were constructed with a Strep-tag II at C-terminal. S2 of WT spike was
404 constructed with a His-tag at C-terminal. Human ACE2 (huACE2, 1-740) was constructed with a
405 Strep-tag II at N-terminal. All recombinant proteins were expressed in FreeStyle 293F cells and
406 purified with Streptactin Agarose Resin 4FF (Yeasen, 20495ES60) or Ni-NTA Agarose (Qiagen,
407 30210).

408 **Cloning and expression of mAbs**

409 As previously described (Li et al., 2023), PBMCs were first incubated with 200nM WT spike. After
410 wash, cells were stained with antibodies targeting CD3, CD19, CD27, CD38, human IgM, human IgD,
411 His-tag and FLAG-tag along with DAPI. WT-spike-specific B cells were gated as $DAPI^-$
412 $CD3^-CD19^+CD27^+IgD^-His^+FLAG^+$ and sorted into 96-well PCR plates with one cell per well. After
413 reverse transcription reaction, variable regions of antibody heavy and light chains from single B cells
414 were amplified by nested PCR and cloned into human IgG1 expression vectors. Paired heavy and
415 light chain plasmids were co-transfected into HEK293T cells or FreeStyle 293F cells. Antibodies were
416 purified with Protein A magnetic beads (GenScript, L00273).

417 **ELISA**

418 Indicated antigens were coated onto 96-well ELISA plates (100 ng/well) at 4˚C overnight. After
419 blocking with blocking buffer (PBS with 10% FBS), undiluted HEK293T supernatant was added to the
420 wells and incubated at 37˚C for 1hr. After wash, HRP-conjugated goat anti-human-IgG antibodies
421 (Zen-bio, 550004) were added and incubated at 37˚C for 1hr. After wash, TMB substrate (Sangon
422 Biotech, E661007-0100) was added and incubated at room temperature for 5 minutes. Then the
423 reaction was stopped with stop solution and absorbance at 450 nm (OD450) was measured.

424 **Pseudovirus neutralization assay**

425 To generate pseudoviruses, HEK293T cells were transfected with psPAX2, pLenti-luciferase and
426 spike-encoding plasmids (WT, Alpha, Beta, Gamma, Delta, BA.1, BA.4/5, BA.2.75, BQ.1, XBB,
427 XBB.1.5, EG.5.1, HK.3, BA.2.86, JN.1, KP.2, KP.3, SARS-CoV-1, Pangolin CoV GD, Bat CoV WIV16,
428 Bat CoV RaTG13 and KP.3 mutants) using polyetherimide (PEI). Pseudoviruses supernatants were
429 collected 48hrs after transfection. 3-fold serially diluted plasma (starting at 1:20), HEK293T
430 supernatant (starting at 1:4.5), or mAbs (starting at 10 μg/ml) were mixed with pseudoviruses at 37˚C
431 for 1hr. HEK293T-hACE2 cells (1.5×10^4 per well) were added into the mixture and incubated at 37˚C
432 for 48hrs. Cells were lysed to measure luciferase activity by Bright-Lite Luciferase Assay System
433 (Vazyme Biotech, DD1204-02). The percentages of neutralization were determined by comparing with
434 the virus control. The data were analyzed and plotted with GraphPad Prism.

435 **Competition ELISA**

436 Purified huACE2, CR3022, S309, P2S-2E9, BD55-5483, BD56-1854 and BD55-1205 were labeled
437 with HRP (ProteinTech, PK20001). WT RBD was coated onto 96-well ELISA plates (50 ng/well). After
438 blocking with blocking buffer (PBS with 10% FBS), blocking mAbs were added and incubated at 37
439 ˚C for 1 hr. Then HRP-labeled detecting reagents were added in the presence of blocking mAbs and
440 incubated at 37˚C for 1 hr. The ratio of blocking and detecting reagents was 100:1. After wash, TMB
441 substrate (Sangon Biotech, E661007-0100) was added and incubated at room temperature for 30
442 minutes. Then the reaction was stopped with stop solution and absorbance at 450 nm (OD450) was
443 measured. The percentages of signal reduction caused by blocking mAbs were calculated.

444 **Binding activity measured by FACS**

445 The plasmids encoding spikes of WT, BA.4/5, KP.3 and KP.3 mutants were transfected into HEK293T
446 cells. After 48hr, cells were harvested. To compare the binding activity of germline and mature

447 antibodies to WT and BA.4/5 spikes, cells were incubated with 3-fold serially diluted germline or
448 mature mAbs (starting at 10 μg/ml) for 30 min at 4˚C. To compare the binding with KP.3 and KP.3
449 mutants, cells were incubated with 1 μg/ml mAbs or 10 nM biotinylated ACE2 for 30 min at 4˚C. After
450 wash, cells stained with mAbs were further stained with DAPI and goat anti-human IgG FITC
451 (Proteintech, SA00003-12), whereas cells stained with ACE2 were further stained with DAPI and
452 streptavidin APC (Biolegend, 405243). After wash, cells were analyzed by CytoFLEX (BECKMAN
453 COULTER). FACS data were analyzed with Flowjo V10 to determine the percentages of positive cells.
454 To compare the binding activity of germline and mature antibodies to WT and BA.4/5 spikes, the
455 percentages were ploted with GraphPad Prism. To compare the binding with KP.3 and KP.3 mutants,
456 the percentages for KP.3 mutants were divided by the percentages for KP.3 and the ratios were
457 recorded.

458 **Sequence analysis**

459 Variable regions of antibody heavy and light chains from single B cells were analyzed with IgBlast
460 (https://www.ncbi.nlm.nih.gov/igblast/). Using Python 3.12, clonotypes were analyzed with the Bio,
461 pandas, and numpy packages. Antibodies with same V and J genes and more than 85% similarity in
462 CDR3 (nucleotide sequence) for both heavy and light chains were defined as clones within the same
463 clonotype. Spike sequences, uploaded from June 1 2024 to October 1 2024, were obtained from
464 NCBI Virus. Sequences with lengths outside the range of 1250–1290 or containing 'X' were removed.
465 Sequence alignment was performed using Muscle5, and statistical analysis was conducted with
466 Python 3.12.

467 **Statistics and reproducibility**

468 All statistical analyses were performed with GraphPad Prism. The numbers of biological repeats for

469 each experiment and tests for statistical significance are described in corresponding figure legends.

470 **Supplemental material**

471 Figures S1–S7

472 Data S1. Excel spreadsheet containing numerical data for figures.

473 **Data Availability Statement**

474 All relevant data are within the manuscript and its supplemental files.

475 **Acknowledgements**

476 The authors thank the donors for providing peripheral blood. The authors thank Professor Linqi Zhang
477 and Peng Chen at Tsinghua University for confirming the pan-sarbecovirus neutralization of IGHV3-
478 74 mAbs, and for providing plasmids encoding spikes of Pangolin CoV GD, Bat CoV WIV16, Bat CoV
479 RaTG13 and plasmids encoding the heavy and light chains of mAb P2S-2E9. This work is supported
480 by the National Key Plan for Scientific Research and Development of China (Grant No.
481 2022YFC2305800) and the National Natural Science Foundation of China (Grant No. 32200765,
482 Grant No. 32370941).

483 **Author contributions**

484 Conceptualization, L.J. and T.Z.; Validation, X.C., L.L., R.D., Z.W.; Formal Analysis, X.C., L.L., R.D.,
485 Z.W. and Y.L.; Investigation, X.C., L.L., R.D., Z.W., Y.L., Y.S., R.Q., H.F., L.H., X.C., M.L., X.H. and
486 L.J.; Writing – Original Draft, X.C., L.L., R.D., Z.W., Y.L., L.J. and T.Z.; Writing – Review & Editing, L.J.
487 and T.Z.; Visualization, X.C., L.L., Z.W. and Y.L.; Supervision, L.J. and T.Z.; Funding Acquisition, L.J.
488 and T.Z..

489 **Competing interests**

490 L.J., T.Z., X.C., L.L., R.D. and Z.W. are inventors on a patent application for antibodies including

KXD350, KXD352, KXD355, KXD358. The other authors have no competing interests.

References

Abramson, J., J. Adler, J. Dunger, R. Evans, T. Green, A. Pritzel, O. Ronneberger, L. Willmore, A.J. Ballard, J. Bambrick, S.W. Bodenstein, D.A. Evans, C.C. Hung, M. O'Neill, D. Reiman, K. Tunyasuvunakool, Z. Wu, A. Zemgulyte, E. Arvaniti, C. Beattie, O. Bertolli, A. Bridgland, A. Cherepanov, M. Congreve, A.I. Cowen-Rivers, A. Cowie, M. Figurnov, F.B. Fuchs, H. Gladman, R. Jain, Y.A. Khan, C.M.R. Low, K. Perlin, A. Potapenko, P. Savy, S. Singh, A. Stecula, A. Thillaisundaram, C. Tong, S. Yakneen, E.D. Zhong, M. Zielinski, A. Zidek, V. Bapst, P. Kohli, M. Jaderberg, D. Hassabis, and J.M. Jumper. 2024. Accurate structure prediction of biomolecular interactions with AlphaFold 3. *Nature* 630:493-500.

Alsoussi, W.B., S.K. Malladi, J.Q. Zhou, Z.M. Liu, B.L. Ying, W. Kim, A.J. Schmitz, T.T. Lei, S.C. Horvath, A.J. Sturtz, K.M. McIntire, B. Evavold, F.J. Han, S.M. Scheaffer, I.F. Fox, S.F. Mirza, L. Parra-Rodriguez, R. Nachbagauer, B. Nestorova, S. Chalkias, C.W. Farnsworth, M.K. Klebert, I. Pusic, B.S. Strnad, W.D. Middleton, S.A. Teefey, S.P.J. Whelan, M.S. Diamond, R. Paris, J.A. O'Halloran, R.M. Presti, J.S. Turner, and A.H. Ellebedy. 2023. SARS-CoV-2 Omicron boosting induces de novo B cell response in humans. *Nature* 617:592-+.

Batista, F.D., and N.E. Harwood. 2009. The who, how and where of antigen presentation to B cells. *Nat Rev Immunol* 9:15-27.

Bruhn, M., M. Obara, A. Salam, B. Costa, A. Ziegler, I. Waltl, A. Pavlou, M. Hoffmann, T. Graalmann, S. Pöhlmann, A. Schambach, and U. Kalinke. 2024. Diversification of the VH3-53 immunoglobulin gene segment by somatic hypermutation results in neutralization of SARS-CoV-2 virus variants. *Eur J Immunol* 54:

Cao, Y.L., F.C. Jian, J. Wang, Y.L. Yu, W.L. Song, A. Yisimayi, J. Wang, R. An, X.S. Chen, N. Zhang, Y. Wang, P. Wang, L.J. Zhao, H.Y. Sun, L.L. Yu, S.J. Yang, X. Niu, T.H. Xiao, Q.Q. Gu, F. Shao, X.H. Hao, Y.L. Xu, R.H. Jin, Z.Y. Shen, Y.C. Wang, and X.S. Xie. 2023. Imprinted SARS-CoV-2 humoral immunity induces convergent Omicron RBD evolution. *Nature* 614:521-+.

Cao, Y.L., F.C. Jian, Z.Y. Zhang, A. Yisimayi, X.H. Hao, L.L. Bao, F. Yuan, Y.L. Yu, S. Du, J. Wang, T.H. Xiao, W.L. Song, Y. Zhang, P.L. Liu, R. An, P. Wang, Y. Wang, S.J. Yang, X. Niu, Y.H. Zhang, Q.Q. Gu, F. Shao, Y.L. Hu, W.D. Yin, A.H. Zheng, Y.C. Wang, C. Qin, R.H. Jin, J.Y. Xiao, and X.L.S. Xie. 2022. Rational identification of potent and broad sarbecovirus-neutralizing antibody cocktails from SARS convalescents. *Cell Reports* 41:

Cerutti, G., Y. Guo, T. Zhou, J. Gorman, M. Lee, M. Rapp, E.R. Reddem, J. Yu, F. Bahna, J. Bimela, Y. Huang, P.S. Katsamba, L. Liu, M.S. Nair, R. Rawi, A.S. Olia, P. Wang, B. Zhang, G.Y. Chuang, D.D. Ho, Z. Sheng, P.D. Kwong, and L. Shapiro. 2021. Potent SARS-CoV-2 neutralizing antibodies directed against spike N-terminal domain target a single supersite. *Cell Host Microbe* 29:819-833 e817.

Gaebler, C., Z. Wang, J.C.C. Lorenzi, F. Muecksch, S. Finkin, M. Tokuyama, A. Cho, M. Jankovic, D. Schaefer-Babajew, T.Y. Oliveira, M. Cipolla, C. Viant, C.O. Barnes, Y. Bram, G. Breton, T. Hagglof, P. Mendoza, A. Hurley, M. Turroja, K. Gordon, K.G. Millard, V. Ramos, F. Schmidt, Y. Weisblum, D. Jha, M. Tankelevich, G. Martinez-Delgado, J. Yee, R. Patel, J. Dizon, C. Unson-O'Brien, I. Shimeliovich, D.F. Robbiani, Z. Zhao, A. Gazumyan, R.E. Schwartz, T. Hatziioannou, P.J. Bjorkman, S. Mehandru, P.D. Bieniasz, M. Caskey, and M.C. Nussenzweig. 2021. Evolution of antibody immunity to SARS-CoV-2. *Nature* 591:639-644.

Hastie, K.M., H. Li, D. Bedinger, S.L. Schendel, S.M. Dennison, K. Li, V. Rayaprolu, X. Yu, C. Mann, M.

533 Zandonatti, R. Diaz Avalos, D. Zyla, T. Buck, S. Hui, K. Shaffer, C. Hariharan, J. Yin, E. Olmedillas, A.
534 Enriquez, D. Parekh, M. Abraha, E. Feeney, G.Q. Horn, V.I.C.D.B.t. Co, Y. Aldon, H. Ali, S. Aracic, R.R.
535 Cobb, R.S. Federman, J.M. Fernandez, J. Glanville, R. Green, G. Grigoryan, A.G. Lujan Hernandez,
536 D.D. Ho, K.A. Huang, J. Ingraham, W. Jiang, P. Kellam, C. Kim, M. Kim, H.M. Kim, C. Kong, S.J. Krebs,
537 F. Lan, G. Lang, S. Lee, C.L. Leung, J. Liu, Y. Lu, A. MacCamy, A.T. McGuire, A.L. Palser, T.H. Rabbitts,
538 Z. Rikhtegaran Tehrani, M.M. Sajadi, R.W. Sanders, A.K. Sato, L. Schweizer, J. Seo, B. Shen, J.L.
539 Snitselaar, L. Stamatatos, Y. Tan, M.T. Tomic, M.J. van Gils, S. Youssef, J. Yu, T.Z. Yuan, Q. Zhang, B.
540 Peters, G.D. Tomaras, T. Germann, and E.O. Saphire. 2021. Defining variant-resistant epitopes
541 targeted by SARS-CoV-2 antibodies: A global consortium study. *Science* 374:472-478.
542 Huang, C.Q., S. Vishwanath, G.W. Carnell, A.C.Y. Chan, and J.L. Heeney. 2023. Immune imprinting and next-
543 generation coronavirus vaccines. *Nat Microbiol* 8:1971-1985.
544 Inoue, T., I. Moran, R. Shinnakasu, T.G. Phan, and T. Kurosaki. 2018. Generation of memory B cells and their
545 reactivation. *Immunol Rev* 283:138-149.
546 Jian, F., J. Wang, A. Yisimayi, W. Song, Y. Xu, X. Chen, X. Niu, S. Yang, Y. Yu, P. Wang, H. Sun, L. Yu, J. Wang,
547 Y. Wang, R. An, W. Wang, M. Ma, T. Xiao, Q. Gu, F. Shao, Y. Wang, Z. Shen, R. Jin, and Y. Cao. 2024.
548 Evolving antibody response to SARS-CoV-2 antigenic shift from XBB to JN.1. *Nature*
549 Johnston, T.S., S.H. Li, M.M. Painter, R.K. Atkinson, N.R. Douek, D.B. Reeg, D.C. Douek, E.J. Wherry, and S.E.
550 Hensley. 2024. Immunological imprinting shapes the specificity of human antibody responses against
551 SARS-CoV-2 variants. *Immunity* 57:912-925 e914.
552 Ju, B., Q. Zhang, Z. Wang, Z.Q. Aw, P. Chen, B. Zhou, R. Wang, X. Ge, Q. Lv, L. Cheng, R. Zhang, Y.H. Wong,
553 H. Chen, H. Wang, S. Shan, X. Liao, X. Shi, L. Liu, J.J.H. Chu, X. Wang, Z. Zhang, and L. Zhang. 2023.
554 Infection with wild-type SARS-CoV-2 elicits broadly neutralizing and protective antibodies against
555 omicron subvariants. *Nat Immunol* 24:690-699.
556 Kaku, C.I., A.J. Bergeron, C. Ahlm, J. Normark, M. Sakharkar, M.N.E. Forsell, and L.M. Walker. 2022. Recall of
557 preexisting cross-reactive B cell memory after Omicron BA.1 breakthrough infection. *Sci Immunol*
558 7:eabq3511.
559 Kaku, C.I., T.N. Starr, P. Zhou, H.L. Dugan, P. Khalife, G. Song, E.R. Champney, D.W. Mielcarz, J.C. Geoghegan,
560 D.R. Burton, R. Andrabi, J.D. Bloom, and L.M. Walker. 2023. Evolution of antibody immunity following
561 Omicron BA.1 breakthrough infection. *Nat Commun* 14:2751.
562 Kim, W., J.Q. Zhou, S.C. Horvath, A.J. Schmitz, A.J. Sturtz, T. Lei, Z. Liu, E. Kalaidina, M. Thapa, W.B. Alsoussi,
563 A. Haile, M.K. Klebert, T. Suessen, L. Parra-Rodriguez, P.A. Mudd, S.P.J. Whelan, W.D. Middleton, S.A.
564 Teefey, I. Pusic, J.A. O'Halloran, R.M. Presti, J.S. Turner, and A.H. Ellebedy. 2022. Germinal centre-
565 driven maturation of B cell response to mRNA vaccination. *Nature* 604:141-145.
566 Korenkov, M., M. Zehner, H. Cohen-Dvashi, A. Borenstein-Katz, L. Kottege, H. Janicki, K. Vanshylla, T. Weber,
567 H. Gruell, M. Koch, R. Diskin, C. Kreer, and F. Klein. 2023. Somatic hypermutation introduces bystander
568 mutations that prepare SARS-CoV-2 antibodies for emerging variants. *Immunity* 56:
569 Kotaki, R., S. Moriyama, S. Oishi, T. Onodera, Y. Adachi, E. Sasaki, K. Ishino, M. Morikawa, H. Takei, H.
570 Takahashi, T. Takano, A. Nishiyama, K. Yumoto, K. Terahara, M. Isogawa, T. Matsumura, M. Shinkai,
571 and Y. Takahashi. 2024. Repeated Omicron exposures redirect SARS-CoV-2-specific memory B cell
572 evolution toward the latest variants. *Sci Transl Med* 16:eadp9927.
573 Lapuente, D., T.H. Winkler, and M. Tenbusch. 2024. B-cell and antibody responses to SARS-CoV-2: infection,
574 vaccination, and hybrid immunity. *Cell Mol Immunol* 21:144-158.
575 Li, L., X. Chen, Z. Wang, Y. Li, C. Wang, L. Jiang, and T. Zuo. 2023. Breakthrough infection elicits hypermutated
576 IGHV3-53/3-66 public antibodies with broad and potent neutralizing activity against SARS-CoV-2

variants including the emerging EG.5 lineages. *PLoS Pathog* 19:e1011856.

Liang, C.Y., S. Raju, Z. Liu, Y. Li, G. Asthagiri Arunkumar, J.B. Case, S.M. Scheaffer, S.J. Zost, C.M. Acreman, M. Gagne, S.F. Andrew, D.C. Carvalho Dos Anjos, K.E. Foulds, J.S. McLellan, J.E. Crowe, Jr., D.C. Douek, S.P.J. Whelan, S.M. Elbashir, D.K. Edwards, and M.S. Diamond. 2024. Imprinting of serum neutralizing antibodies by Wuhan-1 mRNA vaccines. *Nature* 630:950-960.

Ling, Z., C. Yi, X. Sun, Z. Yang, and B. Sun. 2023. Broad strategies for neutralizing SARS-CoV-2 and other human coronaviruses with monoclonal antibodies. *Sci China Life Sci* 66:658-678.

Liu, H., and I.A. Wilson. 2022. Protective neutralizing epitopes in SARS-CoV-2. *Immunol Rev* 310:76-92.

McCallum, M., A. De Marco, F.A. Lempp, M.A. Tortorici, D. Pinto, A.C. Walls, M. Beltramello, A. Chen, Z. Liu, F. Zatta, S. Zepeda, J. di Iulio, J.E. Bowen, M. Montiel-Ruiz, J. Zhou, L.E. Rosen, S. Bianchi, B. Guarino, C.S. Fregni, R. Abdelnabi, S.C. Foo, P.W. Rothlauf, L.M. Bloyet, F. Benigni, E. Cameroni, J. Neyts, A. Riva, G. Snell, A. Telenti, S.P.J. Whelan, H.W. Virgin, D. Corti, M.S. Pizzuto, and D. Veesler. 2021. N-terminal domain antigenic mapping reveals a site of vulnerability for SARS-CoV-2. *Cell* 184:2332-2347 e2316.

Paciello, I., G. Pierleoni, E. Pantano, G. Antonelli, P. Pileri, G. Maccari, D. Cardamone, G. Realini, F. Perrone, M.M. Neto, S. Pozzessere, M. Fabbiani, F. Panza, I. Rancan, M. Tumbarello, F. Montagnani, D. Medini, P. Maes, N. Temperton, E. Simon-Loriere, O. Schwartz, R. Rappuoli, and E. Andreano. 2024. Antigenic sin and multiple breakthrough infections drive converging evolution of COVID-19 neutralizing responses. *Cell Rep* 43:114645.

Pinto, D., Y.J. Park, M. Beltramello, A.C. Walls, M.A. Tortorici, S. Bianchi, S. Jaconi, K. Culap, F. Zatta, A. De Marco, A. Peter, B. Guarino, R. Spreafico, E. Cameroni, J.B. Case, R.E. Chen, C. Havenar-Daughton, G. Snell, A. Telenti, H.W. Virgin, A. Lanzavecchia, M.S. Diamond, K. Fink, D. Veesler, and D. Corti. 2020. Cross-neutralization of SARS-CoV-2 by a human monoclonal SARS-CoV antibody. *Nature* 583:290-295.

Qi, H., B. Liu, X. Wang, and L. Zhang. 2022. The humoral response and antibodies against SARS-CoV-2 infection. *Nat Immunol* 23:1008-1020.

Quandt, J., A. Muik, N. Salisch, B.G. Lui, S. Lutz, K. Kruger, A.K. Wallisch, P. Adams-Quack, M. Bacher, A. Finlayson, O. Ozhelvaci, I. Vogler, K. Grikscheit, S. Hoehl, U. Goetsch, S. Ciesek, O. Tureci, and U. Sahin. 2022. Omicron BA.1 breakthrough infection drives cross-variant neutralization and memory B cell formation against conserved epitopes. *Sci Immunol* 7:eabq2427.

Rao, X., R.C. Zhao, Z. Tong, S.X. Guo, W.Y. Peng, K.F. Liu, S.H. Li, L.L. Wu, J.Y. Tong, Y. Chai, P. Han, F.R. Wang, P. Jia, Z.H. Li, X. Zhao, D.D. Li, R. Zhang, X. Zhang, W.W. Zou, W.W. Li, Q.H. Wang, G.F. Gao, Y. Wu, L.P. Dai, and F. Gao. 2023. Defining a de novo non- RBM antibody as RBD-8 and its synergistic rescue of immune- evaded antibodies to neutralize Omicron SARS- CoV-2. *P Natl Acad Sci USA* 120:

Robbiani, D.F., C. Gaebler, F. Muecksch, J.C.C. Lorenzi, Z. Wang, A. Cho, M. Agudelo, C.O. Barnes, A. Gazumyan, S. Finkin, T. Hagglof, T.Y. Oliveira, C. Viant, A. Hurley, H.H. Hoffmann, K.G. Millard, R.G. Kost, M. Cipolla, K. Gordon, F. Bianchini, S.T. Chen, V. Ramos, R. Patel, J. Dizon, I. Shimeliovich, P. Mendoza, H. Hartweger, L. Nogueira, M. Pack, J. Horowitz, F. Schmidt, Y. Weisblum, E. Michailidis, A.W. Ashbrook, E. Waltari, J.E. Pak, K.E. Huey-Tubman, N. Koranda, P.R. Hoffman, A.P. West, Jr., C.M. Rice, T. Hatziioannou, P.J. Bjorkman, P.D. Bieniasz, M. Caskey, and M.C. Nussenzweig. 2020. Convergent antibody responses to SARS-CoV-2 in convalescent individuals. *Nature* 584:437-442.

Roltgen, K., and S.D. Boyd. 2024. Antibody and B Cell Responses to SARS-CoV-2 Infection and Vaccination: The End of the Beginning. *Annu Rev Pathol* 19:69-97.

Sakharkar, M., C.G. Rappazzo, W.F. Wieland-Alter, C.L. Hsieh, D. Wrapp, E.S. Esterman, C.I. Kaku, A.Z. Wec,

621 J.C. Geoghegan, J.S. McLellan, R.I. Connor, P.F. Wright, and L.M. Walker. 2021. Prolonged evolution
622 of the human B cell response to SARS-CoV-2 infection. *Sci Immunol* 6:
623 Sokal, A., G. Barba-Spaeth, L. Hunault, I. Fernandez, M. Broketa, A. Meola, S. Fourati, I. Azzaoui, A.
624 Vandenberghe, P. Lagouge-Roussey, M. Broutin, A. Roeser, M. Bouvier-Alias, E. Crickx, L. Languille,
625 M. Fournier, M. Michel, B. Godeau, S. Gallien, G. Melica, Y. Nguyen, F. Canoui-Poitrine, F. Pirenne, J.
626 Megret, J.M. Pawlotsky, S. Fillatreau, C.A. Reynaud, J.C. Weill, F.A. Rey, P. Bruhns, M. Mahevas, and
627 P. Chappert. 2023. SARS-CoV-2 Omicron BA.1 breakthrough infection drives late remodeling of the
628 memory B cell repertoire in vaccinated individuals. *Immunity* 56:2137-2151 e2137.
629 Sokal, A., P. Chappert, G. Barba-Spaeth, A. Roeser, S. Fourati, I. Azzaoui, A. Vandenberghe, I. Fernandez, A.
630 Meola, M. Bouvier-Alias, E. Crickx, A. Beldi-Ferchiou, S. Hue, L. Languille, M. Michel, S. Baloul, F.
631 Noizat-Pirenne, M. Luka, J. Megret, M. Menager, J.M. Pawlotsky, S. Fillatreau, F.A. Rey, J.C. Weill, C.A.
632 Reynaud, and M. Mahevas. 2021. Maturation and persistence of the anti-SARS-CoV-2 memory B cell
633 response. *Cell* 184:1201-1213 e1214.
634 Tonegawa, S. 1983. Somatic generation of antibody diversity. *Nature* 302:575-581.
635 Tortorici, M.A., A. Addetia, A.J. Seo, J. Brown, K. Sprouse, J. Logue, E. Clark, N. Franko, H. Chu, and D. Veesler.
636 2024. Persistent immune imprinting occurs after vaccination with the COVID-19 XBB.1.5 mRNA booster
637 in humans. *Immunity* 57:904-911 e904.
638 Turner, J.S., J.A. O'Halloran, E. Kalaidina, W. Kim, A.J. Schmitz, J.Q. Zhou, T. Lei, M. Thapa, R.E. Chen, J.B.
639 Case, F. Amanat, A.M. Rauseo, A. Haile, X. Xie, M.K. Klebert, T. Suessen, W.D. Middleton, P.Y. Shi, F.
640 Krammer, S.A. Teefey, M.S. Diamond, R.M. Presti, and A.H. Ellebedy. 2021. SARS-CoV-2 mRNA
641 vaccines induce persistent human germinal centre responses. *Nature* 596:109-113.
642 Viana, R., S. Moyo, D.G. Amoako, H. Tegally, C. Scheepers, C.L. Althaus, U.J. Anyaneji, P.A. Bester, M.F. Boni,
643 M. Chand, W.T. Choga, R. Colquhoun, M. Davids, K. Deforche, D. Doolabh, L. du Plessis, S.
644 Engelbrecht, J. Everatt, J. Giandhari, M. Giovanetti, D. Hardie, V. Hill, N.Y. Hsiao, A. Iranzadeh, A. Ismail,
645 C. Joseph, R. Joseph, L. Koopile, S.L. Kosakovsky Pond, M.U.G. Kraemer, L. Kuate-Lere, O. Laguda-
646 Akingba, O. Lesetedi-Mafoko, R.J. Lessells, S. Lockman, A.G. Lucaci, A. Maharaj, B. Mahlangu, T.
647 Maponga, K. Mahlakwane, Z. Makatini, G. Marais, D. Maruapula, K. Masupu, M. Matshaba, S. Mayaphi,
648 N. Mbhele, M.B. Mbulawa, A. Mendes, K. Mlisana, A. Mnguni, T. Mohale, M. Moir, K. Moruisi, M.
649 Mosepele, G. Motsatsi, M.S. Motswaledi, T. Mphoyakgosi, N. Msomi, P.N. Mwangi, Y. Naidoo, N. Ntuli,
650 M. Nyaga, L. Olubayo, S. Pillay, B. Radibe, Y. Ramphal, U. Ramphal, J.E. San, L. Scott, R. Shapiro, L.
651 Singh, P. Smith-Lawrence, W. Stevens, A. Strydom, K. Subramoney, N. Tebeila, D. Tshiabuila, J. Tsui,
652 S. van Wyk, S. Weaver, C.K. Wibmer, E. Wilkinson, N. Wolter, A.E. Zarebski, B. Zuze, D. Goedhals, W.
653 Preiser, F. Treurnicht, M. Venter, C. Williamson, O.G. Pybus, J. Bhiman, A. Glass, D.P. Martin, A.
654 Rambaut, S. Gaseitsiwe, A. von Gottberg, and T. de Oliveira. 2022. Rapid epidemic expansion of the
655 SARS-CoV-2 Omicron variant in southern Africa. *Nature* 603:679-686.
656 Victora, G.D., and M.C. Nussenzweig. 2022. Germinal Centers. *Annu Rev Immunol* 40:413-442.
657 Wang, Q., Y. Guo, A.R. Tam, R. Valdez, A. Gordon, L. Liu, and D.D. Ho. 2023a. Deep immunological imprinting
658 due to the ancestral spike in the current bivalent COVID-19 vaccine. *Cell Rep Med* 4:101258.
659 Wang, Q., Y.C. Guo, R.M. Zhang, J.R. Ho, H. Mohri, R. Valdez, D.M. Manthei, A. Gordon, L.H. Liu, and D.V. Ho.
660 2023b. Antibody neutralisation of emerging SARS- CoV-2 subvariants: EG.5.1 and XBC.1.6. *Lancet*
661 *Infect Dis* 23:E397-E398.
662 Wang, Y., M. Yuan, H. Lv, J. Peng, I.A. Wilson, and N.C. Wu. 2022a. A large-scale systematic survey reveals
663 recurring molecular features of public antibody responses to SARS-CoV-2. *Immunity* 55:1105-1117
664 e1104.

Wang, Z., L. Li, R. Du, X. Chen, Y. Sun, R. Qin, Y. Li, H. Feng, L. Hu, X. Chen, M. Lu, L. Jiang, and T. Zuo. 2024. Ancestral SARS-CoV-2 immune imprinting persists on RBD but not NTD after sequential Omicron infections. *bioRxiv*. doi.org/10.1101/2024.05.30.596664 (Preprint posted July 04, 2024)

Wang, Z., F. Schmidt, Y. Weisblum, F. Muecksch, C.O. Barnes, S. Finkin, D. Schaefer-Babajew, M. Cipolla, C. Gaebler, J.A. Lieberman, T.Y. Oliveira, Z. Yang, M.E. Abernathy, K.E. Huey-Tubman, A. Hurley, M. Turroja, K.A. West, K. Gordon, K.G. Millard, V. Ramos, J. Da Silva, J. Xu, R.A. Colbert, R. Patel, J. Dizon, C. Unson-O'Brien, I. Shimeliovich, A. Gazumyan, M. Caskey, P.J. Bjorkman, R. Casellas, T. Hatziioannou, P.D. Bieniasz, and M.C. Nussenzweig. 2021. mRNA vaccine-elicited antibodies to SARS-CoV-2 and circulating variants. *Nature* 592:616-622.

Wang, Z., P. Zhou, F. Muecksch, A. Cho, T. Ben Tanfous, M. Canis, L. Witte, B. Johnson, R. Raspe, F. Schmidt, E. Bednarski, J. Da Silva, V. Ramos, S. Zong, M. Turroja, K.G. Millard, K.H. Yao, I. Shimeliovich, J. Dizon, A. Kaczynska, M. Jankovic, A. Gazumyan, T.Y. Oliveira, M. Caskey, C. Gaebler, P.D. Bieniasz, T. Hatziioannou, and M.C. Nussenzweig. 2022b. Memory B cell responses to Omicron subvariants after SARS-CoV-2 mRNA breakthrough infection in humans. *J Exp Med* 219:

Weber, T., S. Dahling, S. Rose, P. Affeldt, K. Vanshylla, L. Ullrich, L. Gieselmann, F. Teipel, H. Gruell, V. Di Cristanziano, D.S. Kim, G. Georgiou, M. Koch, C. Kreer, and F. Klein. 2023. Enhanced SARS-CoV-2 humoral immunity following breakthrough infection builds upon the preexisting memory B cell pool. *Sci Immunol* 8:eadk5845.

Yan, Q., R. Hou, X. Huang, Y. Zhang, P. He, Y. Zhang, B. Liu, Q. Wang, H. Rao, X. Chen, X. Zhao, X. Niu, J. Zhao, X. Xiong, and L. Chen. 2022. Shared IGHV1-69-encoded neutralizing antibodies contribute to the emergence of L452R substitution in SARS-CoV-2 variants. *Emerg Microbes Infect* 11:2749-2761.

Yisimayi, A., W. Song, J. Wang, F. Jian, Y. Yu, X. Chen, Y. Xu, S. Yang, X. Niu, T. Xiao, J. Wang, L. Zhao, H. Sun, R. An, N. Zhang, Y. Wang, P. Wang, L. Yu, Z. Lv, Q. Gu, F. Shao, R. Jin, Z. Shen, X.S. Xie, Y. Wang, and Y. Cao. 2024. Repeated Omicron exposures override ancestral SARS-CoV-2 immune imprinting. *Nature* 625:148-156.

Yuan, M., H. Liu, N.C. Wu, C.D. Lee, X. Zhu, F. Zhao, D. Huang, W. Yu, Y. Hua, H. Tien, T.F. Rogers, E. Landais, D. Sok, J.G. Jardine, D.R. Burton, and I.A. Wilson. 2020a. Structural basis of a shared antibody response to SARS-CoV-2. *Science* 369:1119-1123.

Yuan, M., N.C. Wu, X. Zhu, C.D. Lee, R.T.Y. So, H. Lv, C.K.P. Mok, and I.A. Wilson. 2020b. A highly conserved cryptic epitope in the receptor binding domains of SARS-CoV-2 and SARS-CoV. *Science* 368:630-633.

697 **Figures and figure legends**

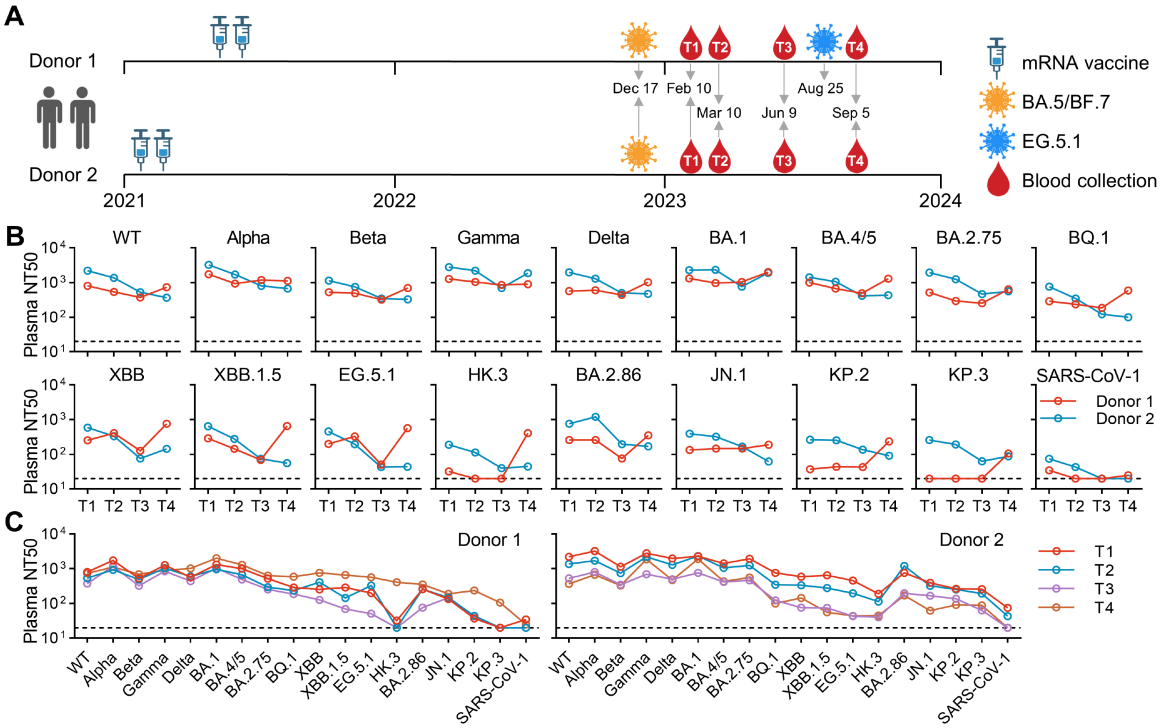

698

699 **Figure 1. Longitudinal analysis of plasma neutralizing antibody responses in two individuals.**

700 (A) Basic information of donors and samples. (B, C) Summary of plasma neutralizing antibody titers

701 (NT50). NT50s are calculated with results from three independent experiments, in which duplicates

702 are performed.

703

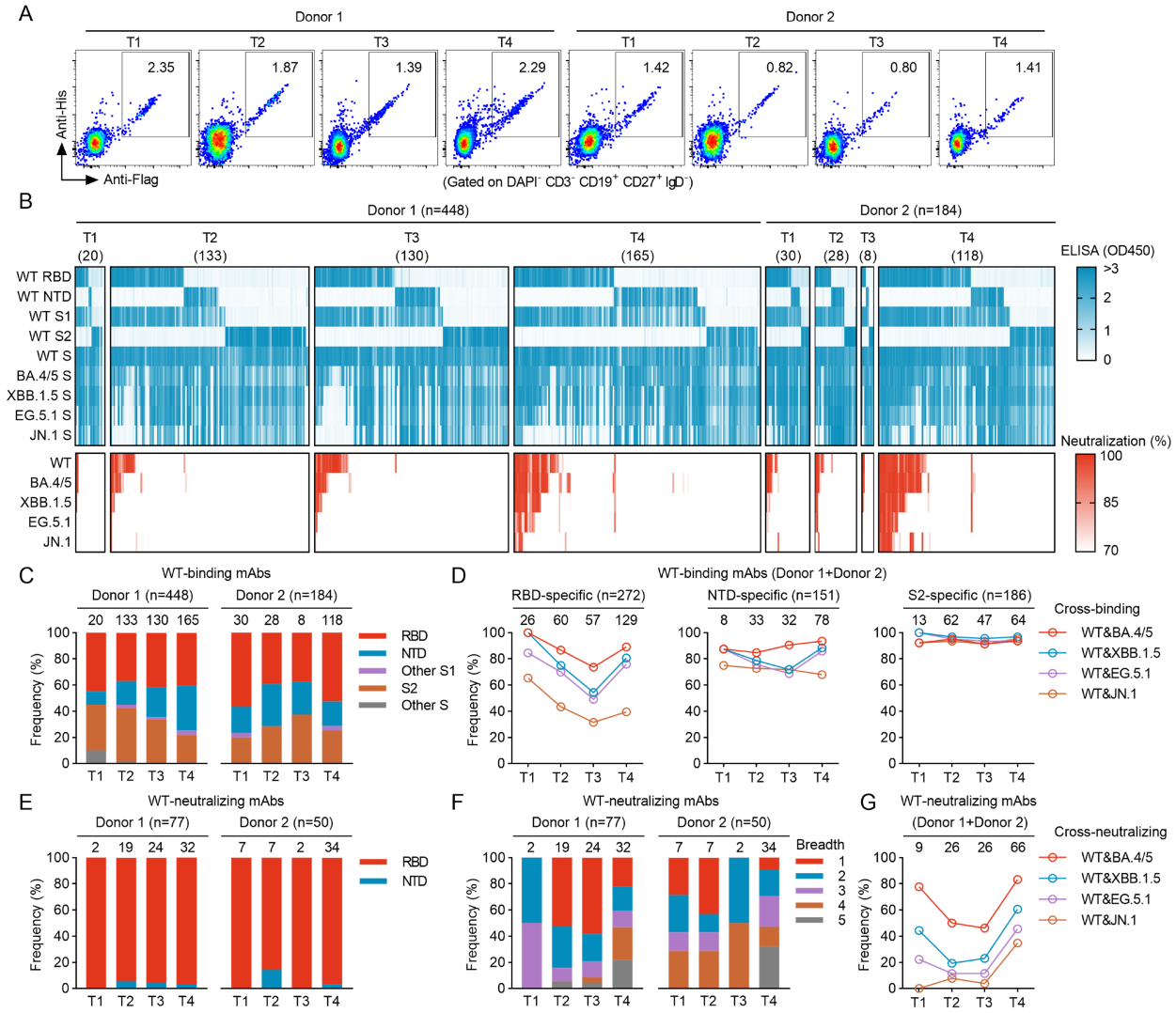

Figure 2. Isolation and characterization of mAbs. (A) FACS plots representing the percentages of WT-spike-specific B cells in DAPI$^-$CD3$^-$CD19$^+$CD27$^+$IgD$^-$ B cells. (B) ELISA and neutralization results of 632 mAbs from two donors. Supernatant of HEK293T is tested against 9 antigens by ELISA, and tested against 5 pseudoviruses by neutralization assay. For ELISA, supernatant is not diluted. For neutralization, supernatant is diluted by 4.5 folds. The results are mean values from two independent experiments, in which duplicates are performed. (C) Frequencies of mAbs targeting each domain among mAbs binding to WT spike (WT-binding mAbs). (D) Frequencies of cross-binding mAbs among RBD-specific, NTD-specific, and S2-specific mAbs. (E) Frequencies of mAbs targeting RBD or NTD among mAbs neutralizing WT pseudoviruses (WT-neutralizing mAbs). (F) Frequencies of mAbs with

714 different neutralizing breadth. Breadth indicates the number of pseudoviruses can be neutralized by

715 mAbs. (G) Frequencies of cross-neutralizing mAbs.

716

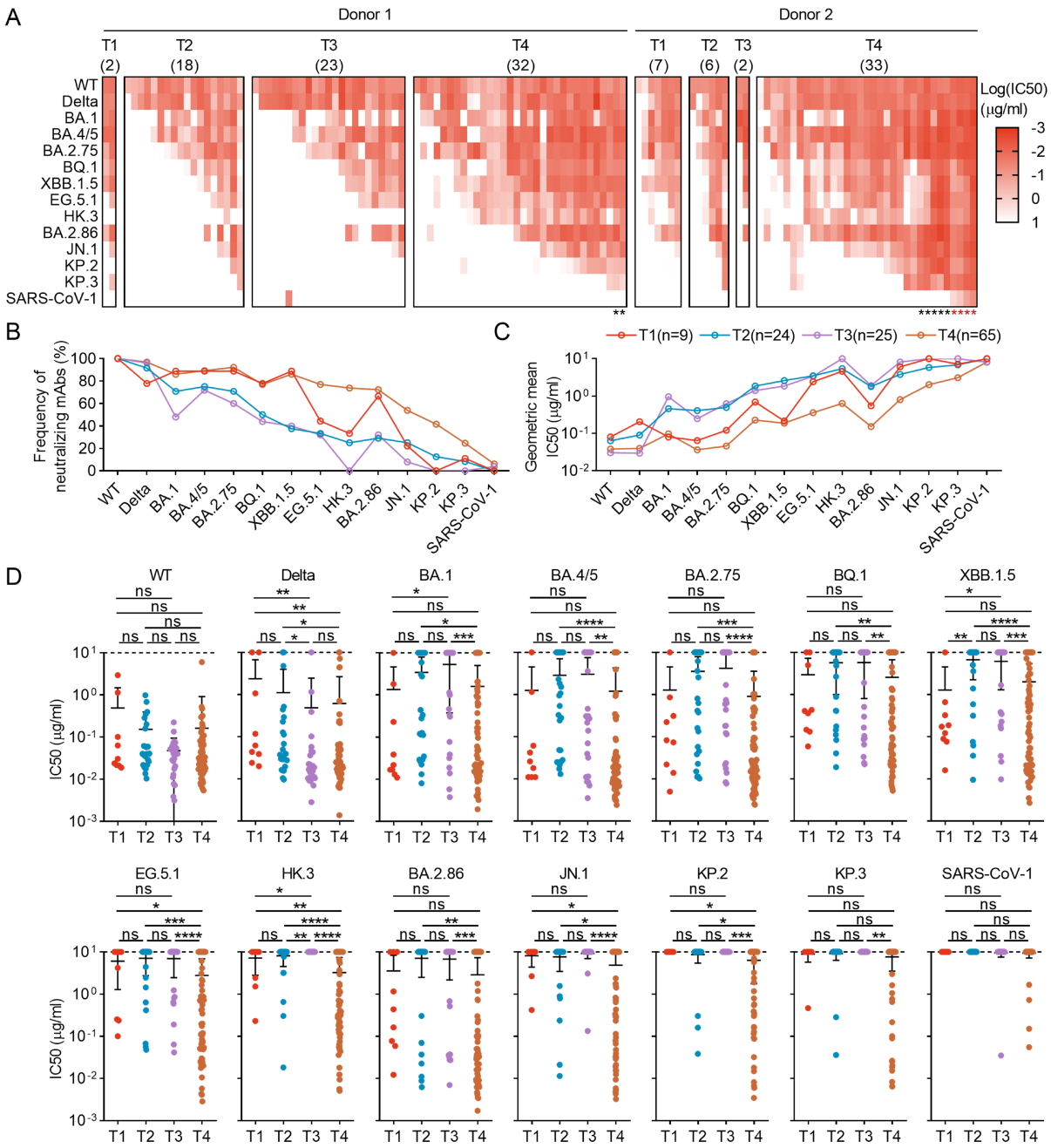

Figure 3. Neutralizing potency of mAbs against SARS-CoV-2 and SARS-CoV-1. (A) IC50s of mAbs against 14 pseudoviruses. The highest antibody concentration used to determine IC50 is 10 μg/ml. IC50s are calculated with results from two independent experiments, in which duplicates are performed. The black asterisk indicates mAbs with broadly neutralizing activity against SARS-CoV-2 variants from WT to KP.3. The red asterisk indicates mAbs with broadly neutralizing activity against SARS-CoV-2 and SARS-CoV-1. (B) Frequencies of neutralizing mAbs against each pseudoviruses

724 among mAbs from T1 to T4. (C) Geometric mean IC50s of mAbs from T1 to T4 against each

725 pseudoviruses. (D) Comparison of IC50s. Statistical analysis is performed by Mann-Whitney test. ns

726 (not significant) $P > 0.05$, *$P < 0.05$, **$P < 0.01$, ***$P < 0.001$, ****$P < 0.0001$.

727

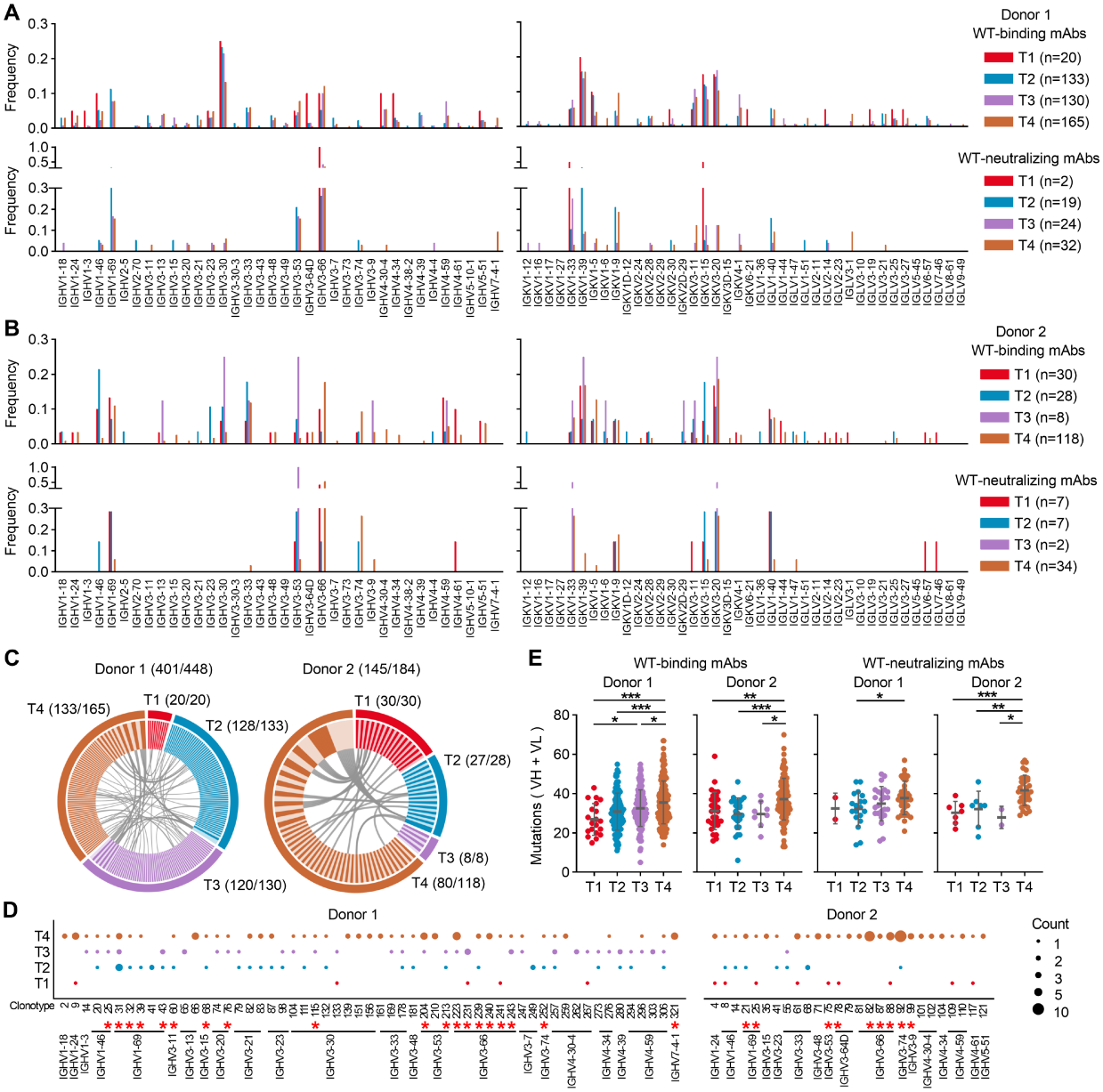

Figure 4. Sequence analysis. (A, B) Frequencies of V genes used by mAbs binding to WT spike (WT-binding mAbs) and mAbs neutralizing WT pseudoviruses (WT-neutralizing mAbs) from Donor 1 and Donor 2. (C) Clonotype analysis of WT-binding mAbs from Donor 1 and Donor 2. Values in parentheses indicate number of clonotypes/number of mAbs. Different clonotypes are distinguished by alternating colors, and identical clonotypes across different time points are connected by gray lines. (D) Bubble plot of clonotypes comprising two or more mAbs. Dot size indicates number of mAbs. The red asterisk indicates clonotypes containing neutralizing mAbs. (E) Somatic hypermutation on

variable regions of heavy and light chains based on DNA sequences. Statistical analysis is performed by two-tailed unpaired T test. *P<0.05, **P < 0.01, ***P < 0.001.

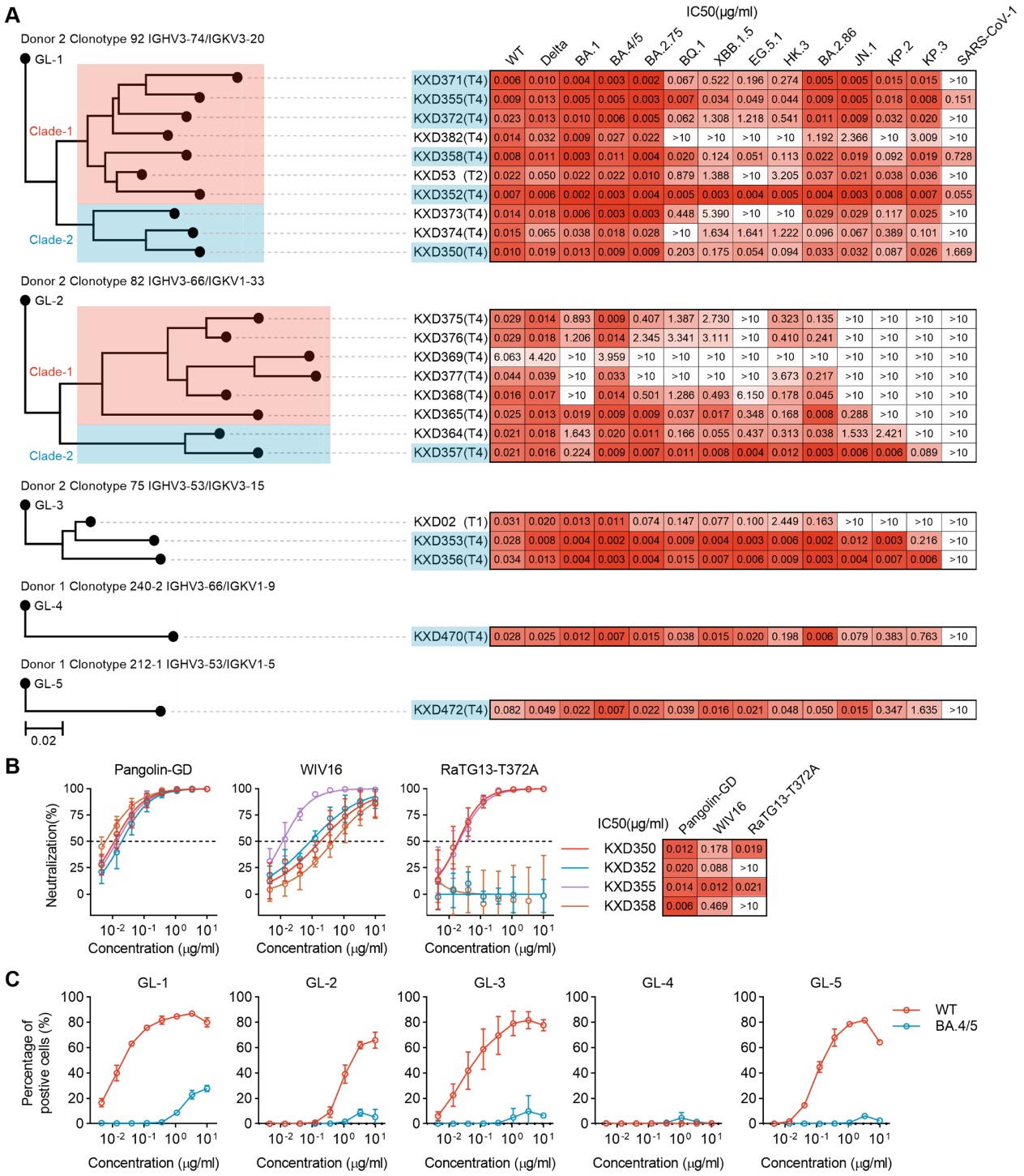

Figure 5. Clonotypes containing mAbs with extraordinary neutralizing breadth and potency. (A) Maximum-likelihood phylogenetic trees of each clonotype and IC50s of each mAbs. (B) Neutralization against sarbecoviruses including Pangolin CoV GD (Pangolin-GD), Bat CoV WIV16 (WIV16) and Bat CoV RaTG13-T372A (RaTG13-T372A). (C) Binding of germline antibodies to WT and BA.4/5 spikes expressed on HEK293T cells.

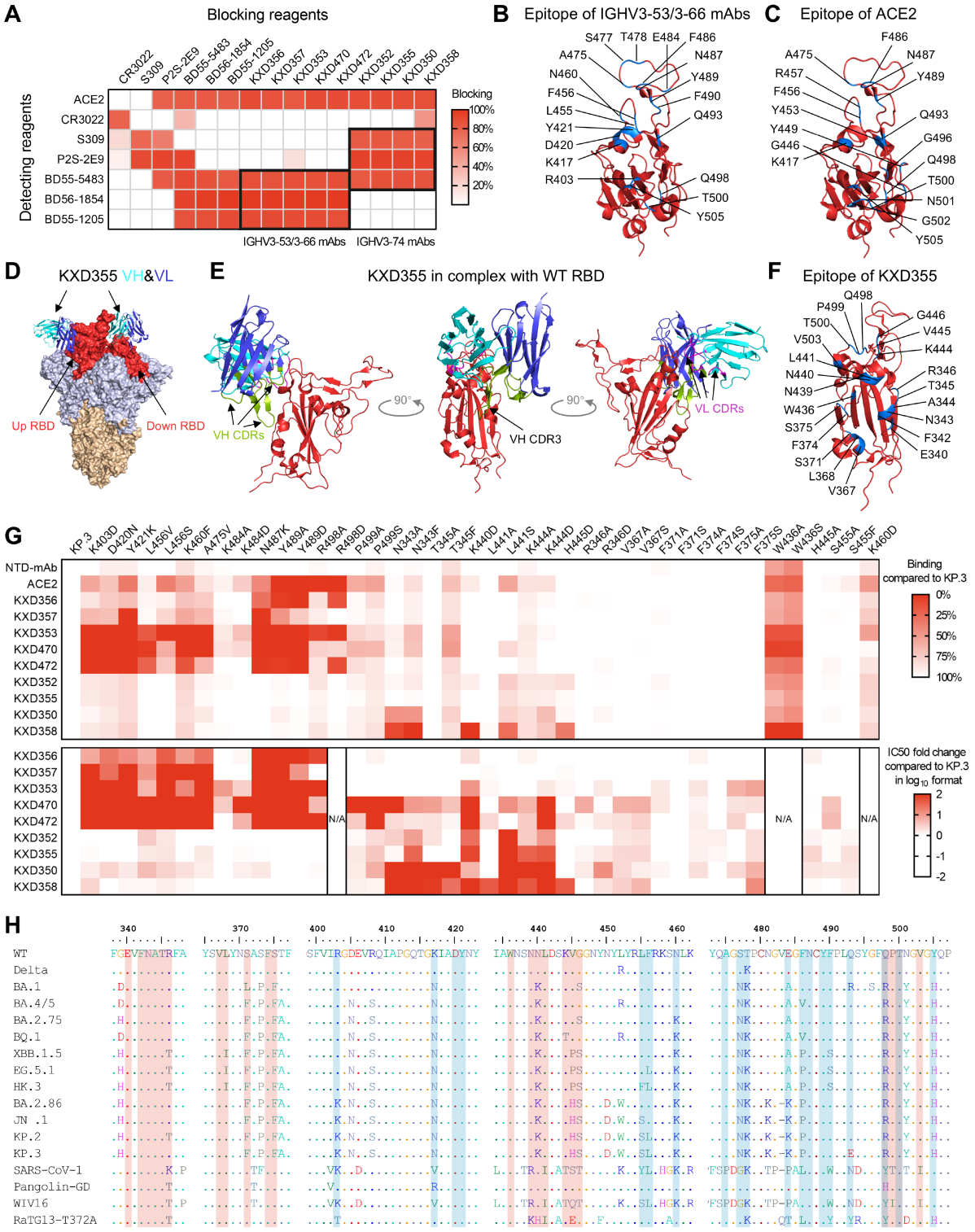

Figure 6. Epitope mapping and escape mutations of mAbs with extraordinary neutralizing breadth and potency. (A) Competition ELISA. The blocking indicates signal (OD450) reduced by blocking mAbs. The results are mean values from two independent experiments, in which duplicates are performed. (B) Epitope of IGHV3-53/3-66 mAbs on WT RBD (PDB: 7A94). (C) Epitope of ACE2

750 on WT RBD (PDB: 7A94). (D) The predicted structure of KXD355 in complex with WT RBD is aligned
751 to up RBD and down RBD on WT spike (PDB: 7A94). (E) Detailed view of KXD355 in complex with
752 WT RBD. (F) Epitope of KXD355 on WT RBD (PDB: 7A94). (G) Binding and neutralizing activities
753 against single-mutated KP.3. The binding activities are measured by FACS. NTD-mAb, a mAb
754 targeting NTD, is used to evaluate the expression levels of KP.3 mutants. The results of binding
755 activities are mean values from two independent experiments. For neutralizing activities, IC50s are
756 calculated with results from two independent experiments, in which duplicates are performed. N/A
757 (not applicable) indicates that neutralization assay is not done because we are not able to generate
758 pseudoviruses for the mutant. (H) Alignment of spike sequences from SARS-CoV-2 variants and other
759 sarbecoviruses tested in neutralization assay. The epitopes of IGHV3-53/3-66 and IGHV3-74 mAbs
760 are respectively highlighted with blue and red background.
761

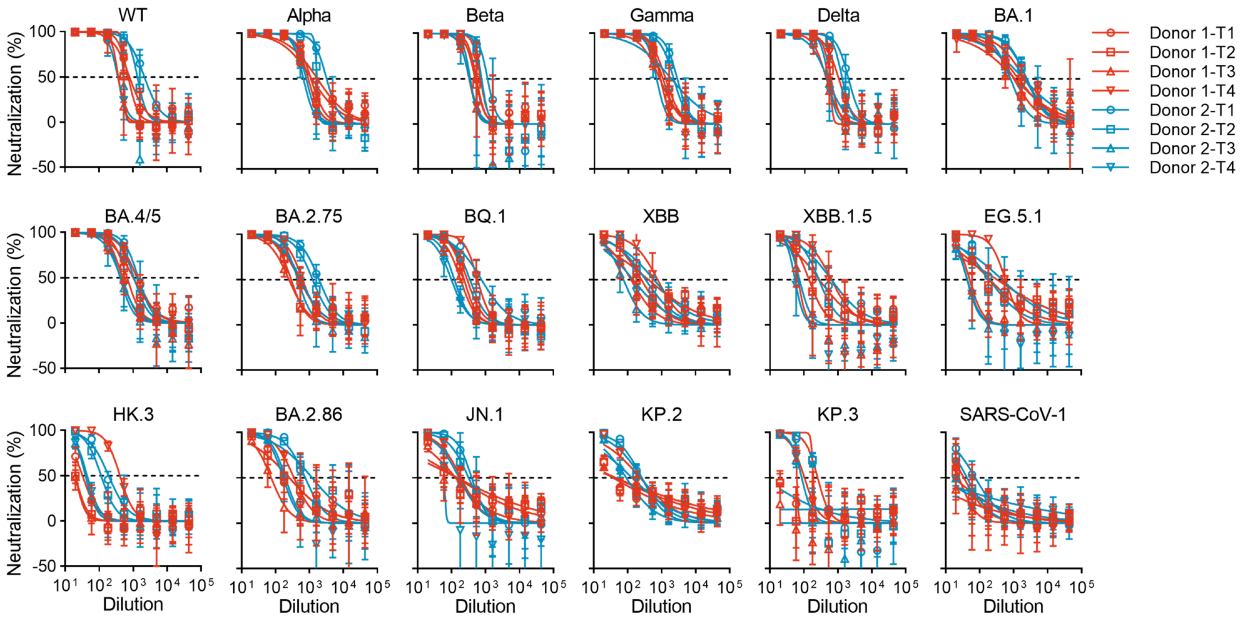

Figure S1. Plasma neutralizing antibody titers. (A) Plasma neutralizing antibody titers against a panel of pseudoviruses. The data are represented as mean ± SD and they are from three independent experiments, in which duplicates are performed. The published data for plasma from T1 are not used here. Instead, we measured the neutralizing tiers of plasma from T1 again, along with plasma from other time points.

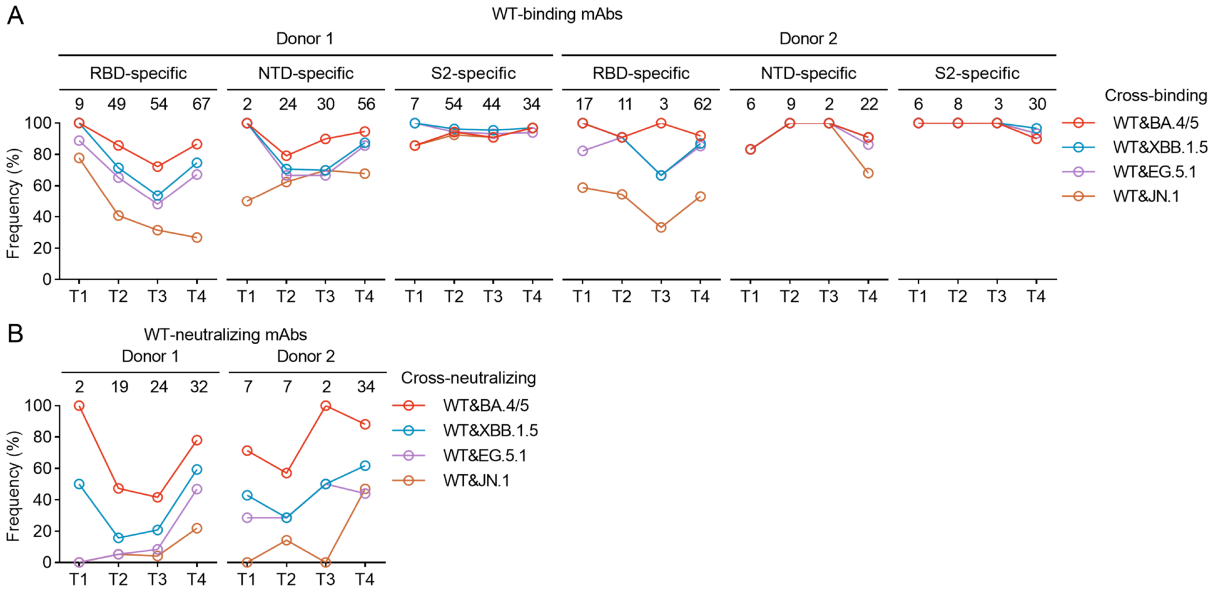

Figure S2. Cross-binding and cross-neutralizing mAbs from Donor 1 and Donor 2. (A) Frequencies of cross-binding mAbs among RBD-specific, NTD-specific, and S2-specific mAbs from Donor 1 and Donor 2. (B) Frequencies of cross-neutralizing mAbs from Donor 1 and Donor 2.

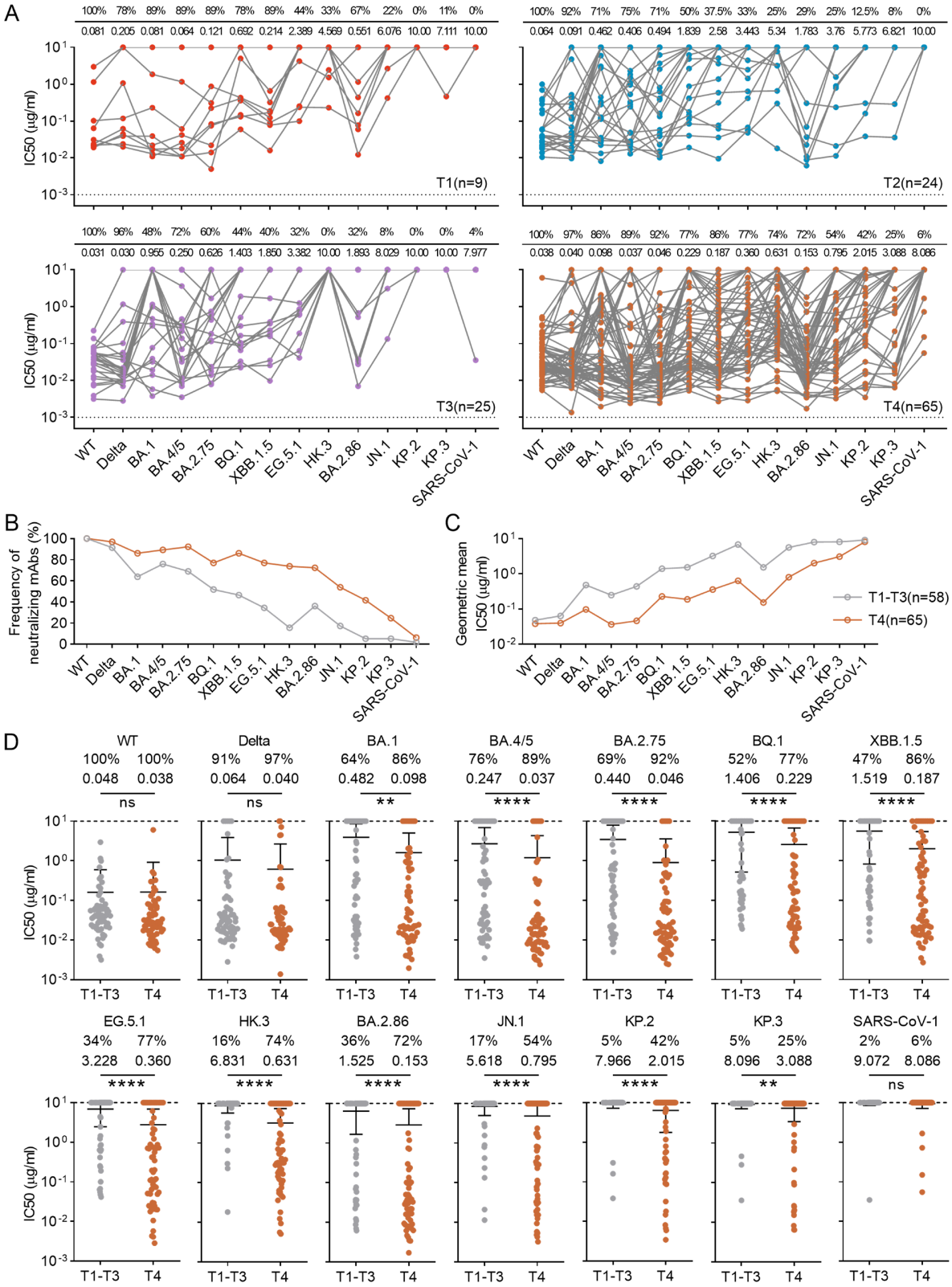

Figure S3. IC50s of mAbs. (A) Summary of IC50s. The numbers below the line indicate the geometric mean IC50s and the numbers above the line represent the percentage of mAbs that is able to

neutralize the corresponding pseudoviruses (IC50 below 10 μg/ml). (B) Frequencies of neutralizing mAbs against each pseudoviruses among T1-T3 group and T4 group. (C) Geometric mean IC50s of mAbs among T1-T3 group and T4 group. (D) Comparison of IC50s. The numbers below and above indicate the geometric mean IC50s and the percentages of neutralizing mAbs, respectively. Statistical analysis is performed by Mann-Whitney test. ns (not significant) $P > 0.05$, **$P < 0.01$, ****$P < 0.0001$.

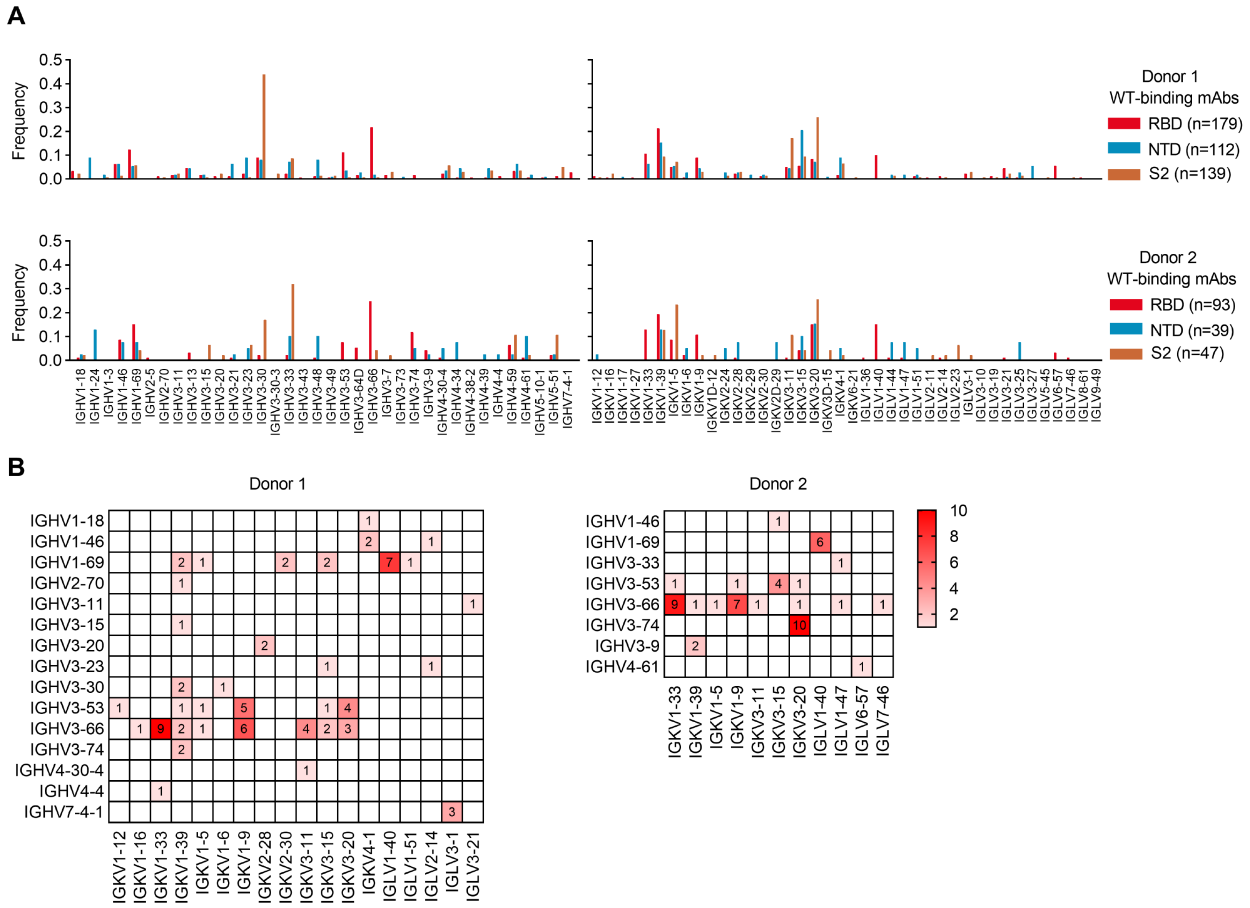

Figure S4. Analysis of V gene usage. (A) Frequencies of V genes used by mAbs targeting RBD, NTD and S2. (B) Paring of V genes for heavy and light chains in neutralizing mAbs. The number in each box indicates the count of mAbs using the corresponding pair.

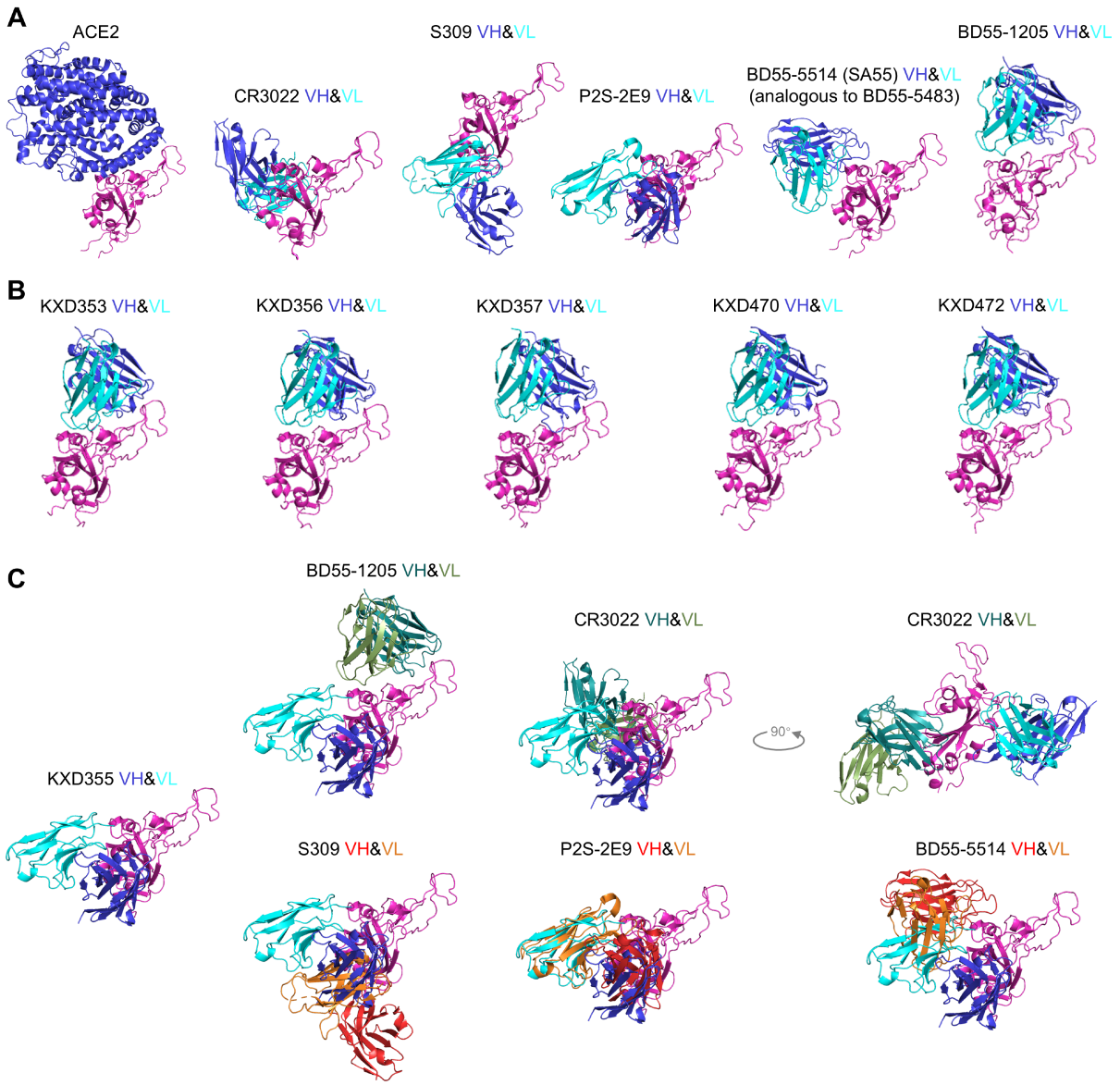

Figure S5. Published structures and predicted structures. (A) The published structures of ACE2 (PDB: 7A94), CR3022 (PDB: 6W41), S309 (PDB: 7TLY), P2S-2E9 (PDB: 7XSA), BD55-5514 (PBD: 7Y0W), BD55-1205 (PDB: 8XEA) in complex with RBD. (B) The predicted structures of KXD353, KXD356, KXD357, KXD470 and KXD472 in complex with WT RBD. (C) The predicted structure of KXD355 in complex with WT RBD is aligned with published structures of CR3022, S309, P2S-2E9, BD55-5514 and BD55-1205.

	KXD356	KXD357	KXD353	KXD470	KXD472	KXD352	KXD355	KXD350	KXD358
KP.3	0.006	0.089	0.216	0.763	1.635	0.007	0.008	0.026	0.019
K403D	0.043	>10	>10	>10	>10	0.006	0.009	0.041	0.05
D420N	0.126	2.407	>10	>10	>10	0.005	0.007	0.067	0.016
Y421K	0.08	>10	>10	>10	>10	0.002	0.005	0.043	0.023
L456V	0.038	0.958	1.114	>10	>10	0.022	0.014	0.117	0.023
L456S	0.243	>10	>10	>10	>10	0.012	0.015	0.072	0.028
K460F	0.057	>10	3.384	>10	>10	0.004	0.008	0.053	0.023
A475V	0.148	>10	>10	>10	>10	0.005	0.013	0.039	0.016
K484A	0.003	0.015	2.174	2.529	1.612	0.003	0.005	0.018	0.006
K484D	0.007	0.03	0.631	>10	9.051	0.005	0.009	0.037	0.012
N487K	>10	>10	>10	>10	>10	0.006	0.008	0.044	0.017
Y489A	>10	>10	>10	>10	>10	0.003	0.002	0.006	0.004
Y489D	>10	0.986	>10	>10	>10	0.001	0.002	0.008	0.002
R498A	0.385	0.017	>10	3.665	>10	0.004	0.006	0.029	0.011
R498D					N/A				
P499A	0.004	0.053	0.086	>10	5.506	0.008	0.013	0.042	0.026
P499S	0.008	0.077	0.195	>10	>10	0.016	0.029	0.162	0.024
N343A	0.003	0.029	0.022	>10	3.81	0.021	0.01	>10	>10
N343F	0.004	0.051	0.061	7.918	2.951	0.063	0.273	>10	>10
T345A	0.004	0.035	0.104	6.648	3.247	0.013	0.005	>10	1.66
T345F	0.003	0.049	0.05	3.132	2.047	0.001	0.001	>10	0.484
K440D	0.013	0.074	2.37	>10	>10	0.191	0.55	0.141	>10
L441A	0.003	0.095	0.263	0.361	3.986	0.004	0.004	0.013	0.852
L441S	0.004	0.066	0.162	9.55	1.348	>10	>10	>10	>10
K444A	0.008	0.048	0.181	4.152	5.256	0.023	0.297	5.636	0.907
K444D	0.003	0.011	0.366	>10	>10	0.072	0.382	>10	>10
H445D	0.003	0.095	0.263	0.361	3.986	0.004	0.004	0.013	0.852
R346A	0.001	0.023	0.164	5.175	1.807	0.002	0.01	0.042	0.019
R346D	0.002	0.009	0.358	0.803	2.898	0.006	0.014	0.35	0.037
V367A	0.005	0.026	0.039	4.553	3.388	0.013	0.02	0.064	0.056
V367S	0.004	0.045	0.071	4.755	4.669	0.014	0.02	0.04	0.103
F371A	0.003	0.017	0.373	1.352	0.94	0.004	0.007	0.033	0.009
F371S	0.003	0.007	0.08	0.303	0.241	0.005	0.005	0.021	0.005
F374A	0.008	0.016	0.385	0.985	2.43	0.01	0.011	0.054	0.018
F374S	0.004	0.006	0.1	0.39	0.293	0.01	0.01	0.019	0.016
F375A	0.004	0.073	1.254	1.477	4.554	0.006	0.007	0.063	0.018
F375S	0.002	0.077	1.785	1.608	1.025	0.015	0.017	0.151	0.266
W436A									
W436S					N/A				
H445A	0.008	0.027	0.134	0.773	0.265	0.009	0.021	0.049	0.02
S455A	0.004	0.062	0.101	2.99	7.856	0.008	0.009	0.045	0.013
S455F	0.005	0.012	0.12	0.621	0.102	0.009	0.016	0.047	0.026
K460D					N/A				

Figure S6. IC50s (μg/ml) against KP.3 mutants.

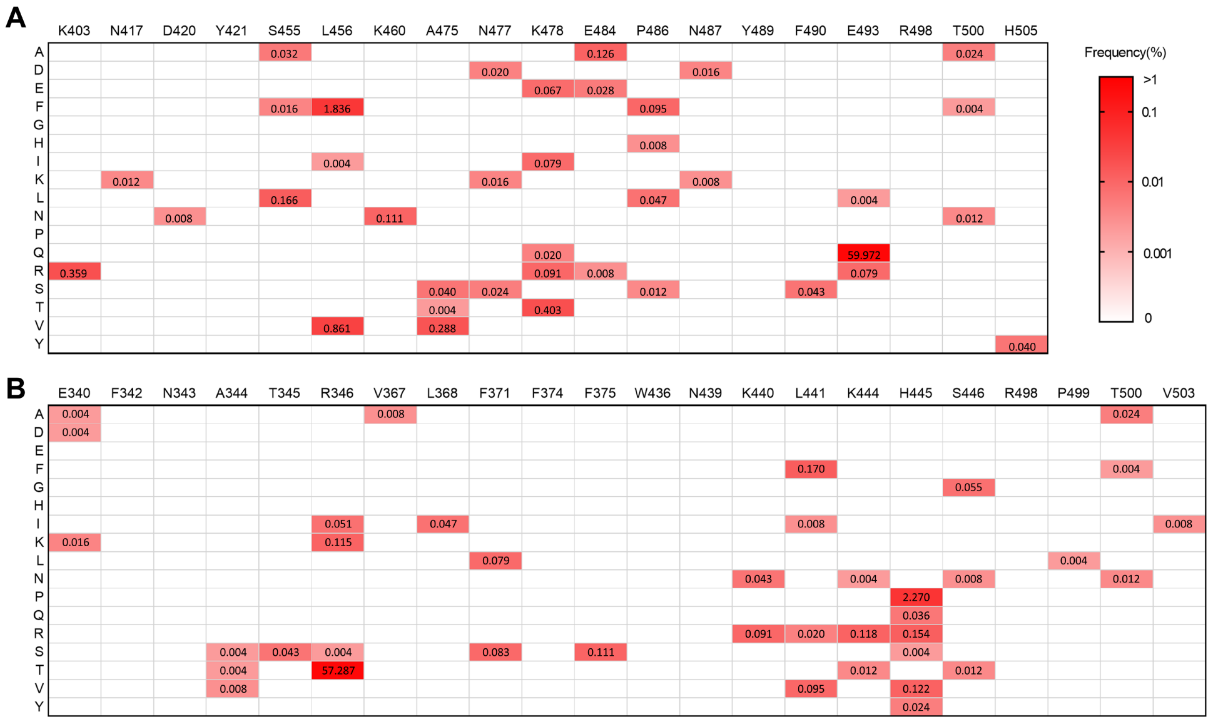

Figure S7. Variations on the epitopes of IGHV3-53/3-66 and IGHV3-74 mAbs. Frequencies of mutations on the epitopes of IGHV3-53/3-66 mAbs (A) and IGHV3-74 mAbs (B) among a total of 25332 spike sequences with KP.3 as reference. The sequences were published between June 1 to October 1 in 2024.